New Absorbing Boundary Conditions and Analytical Model for Multilayered Mushroom-Type Metamaterials: Applications to Wideband Absorbers

Yashwanth R. Padooru, *Student Member, IEEE*, Alexander B. Yakovlev, *Senior Member, IEEE*, Chandra S. R. Kaipa, *Student Member, IEEE*, George W. Hanson, *Fellow, IEEE*, Francisco Medina, *Fellow, IEEE*, Francisco Mesa, *Senior Member, IEEE*, and Allen W. Glisson, *Fellow, IEEE*

***Abstract*—An analytical model is presented for the analysis of multilayer wire media loaded with 2-D arrays of thin material terminations, characterized in general by a complex surface conductivity. This includes the cases of resistive, thin metal, or graphene patches and impedance ground planes. The model is based on the nonlocal homogenization of the wire media with additional boundary conditions (ABCs) at the connection of thin (resistive) material. Based on charge conservation, new ABCs are derived for the interface of two uniaxial wire mediums with thin imperfect conductors at the junction. To illustrate the application of the analytical model and to validate the new ABCs, we characterize the reflection properties of multilayer absorbing structures. It is shown that in such configurations the presence of vias results in the enhancement of the absorption bandwidth and an improvement in the absorptivity performance for increasing angles of an obliquely incident TM-polarized plane wave. The results obtained using the analytical model are validated against full-wave numerical simulations.**

***Index Terms*—Absorbing boundary conditions, dispersive media, electromagnetic scattering by absorbing media, impedance boundary conditions, multilayered media, resistive sheets.**

I. Introduction

In recent years, characterization of metamaterial structures that constitute wire media has attracted special attention, due to their ability in enabling anomalous phenomena such as negative refraction [1], [2] and sub-wavelength imaging [3], [4], among others. However, it has been recently shown in [5] that wire media exhibits strong spatial dispersion at microwave frequencies, and that the constitutive relations between the macroscopic fields and the electric dipole moment are non-local [6]. In [7]–[10], the role of spatial dispersion has been discussed, and it was demonstrated that nonlocal homogenization methods with additional boundary conditions become essential in solving the reflection and transmission problems associated with wire media. Spatially dispersive materials have some advantages that can be successfully exploited for imaging with super resolution [3] and the realization of impedance surfaces [7], among others. However, they can be ineffective for certain applications involving negative refraction [11].

Recently, mushroom structures composed of metallic patches [12] have been shown to suppress (or significantly reduce) spatial dispersion in wire media [13]–[16]. This is because the presence of metallic patches at the wire ends diminishes charge buildup in such a way that, upon homogenization, the mushroom structure can be treated as a uniaxial continuous Epsilon-Negative (ENG) material loaded with a capacitive grid of patches. However, this is not the case when the patches are thin (resistive), where charge accumulation and diffusion at the wire-to-patch interface becomes important, and spatial dispersion effects have to be considered, necessitating an additional boundary condition at this interface [17]. Upon homogenization, these charge effects are reflected in the nonlocal slab permittivity.

It is also observed that for some specific values of the thickness (or resistivity) of the thin material patch, the structure acts as an absorber for obliquely incident TM-polarized plane waves. Electromagnetic absorbing structures have been of interest for a long time due to their ability to reduce the radar cross-section (RCS) of an object at microwave frequencies. The conventional radar absorbers include Salisbury [18] and Jaumann [19] absorbers, which employ either one or more resistive sheets stacked over each other at a distance of a quarter wavelength (measured at the center frequency of the absorption band). However, due to relatively large thickness, these absorbers are inadequate in practical applications such as stealth technology for aircraft, missiles, and other vehicles.

Recently, a renewed interest has arisen in designing electrically thin absorbers based on metamaterials [20]–[28] and high impedance surfaces (HIS) [29]–[32]. These structures are artificially engineered materials having various metallic inclusions with dimensions of order $\lambda/10 - \lambda/4$. In particular, the absorbers based on metamaterials can be scaled from microwave [20], [21] to terahertz [22]–[24], infrared [25], [26], and even to optical [27] regimes through careful design of the constituent inclusions.

Manuscript received January 21, 2012; revised April 24, 2012; accepted July 02, 2012. Date of publication July 18, 2012; date of current version November 29, 2012. This work was supported iin part by the NASA/MS Space Grant Consortium Research Infrastructure Program (project NG05GJ72H), in part by the Spanish Ministerio de Ciencia e Innovación and European Union FEDER funds (projects TEC2010-16948 and CSD2008-00066), and in part by Junta de Andalucía (project P09-TIC-4595).

Y. R. Padooru, A. B. Yakovlev, C. S. R. Kaipa and A. W. Glisson are with the Department of Electrical Engineering, The University of Mississippi, University, MS 38677 USA (e-mail: ypadooru@olemiss.edu, yakovlev@olemiss.edu, ckaipa@olemiss.edu, aglisson@olemiss.edu).

G. W. Hanson is with the Department of Electrical Engineering and Computer Science, University of Wisconsin-Milwaukee, Milwaukee, WI 53211 USA (e-mail: george@uwm.edu).

F. Medina is with the Department of Electronics and Electromagnetism, University of Seville, Seville 41012, Spain (e-mail: medina@us.es).

F. Mesa is with the Department of Applied Physics 1, University of Seville, Seville 41012, Spain (e-mail: mesa@us.es).

Color versions of one or more of the figures in this paper are available online at http://ieeexplore.ieee.org.

Digital Object Identifier 10.1109/TAP.2012.2209196

The common feature of all of the above single-layer metamaterial and HIS absorbers is that they operate in a single narrow frequency band with high absorption at a specific frequency. One possible way to extend the bandwidth is to use Jaumann absorbers [19] mentioned above. Further improvement in the bandwidth of the Jaumann absorber can be achieved by replacing the homogeneous resistive sheets with lossy band-stop resonating frequency selective surfaces (FSS), resulting in circuit analog (CA) absorbers [33], [34]. Also in [35] and [36] the capacitive circuit absorber (CCA) method has been proposed for the design of absorbers with large bandwidths and optimal thicknesses in comparison to the Jaumann and CA absorbers. Most of the design procedures of the Jaumann and CA absorbers have been formulated for normal angle of incidence. Only a few design methods have been published considering oblique angle of incidence for different polarizations [37]–[39]. In [38] and [39], absorbing structures based on a single-layer mushroom HIS consisting of PEC patches placed on top of a metal backed wire-medium slab have been considered. However, these designs behave as materials with a local response, and the absorption is due to a lossy dielectric slab [39] or a resistive sheet placed on top of the structure [38]. Also, in [39] it has been shown that the presence of vias enhances the absorption bandwidth for obliquely incident TM-polarized plane waves.

Most of the absorbers are analyzed using time-consuming brute-force numerical simulations [40], [41], which do not provide much physical insight into the problem. Recently, homogenization methods [42]–[46] have been proposed to avoid the extensive computations demanded by the numerical simulations. These methods are shown to be very effective in modeling the interaction of electromagnetic waves with artificial materials formed by lattices of periodic metallic or magneto-dielectric inclusions, and can be performed almost instantaneously.

In this paper we extend our model [17] (wherein a single-layer mushroom structure with imperfectly conducting patches was considered) to study the absorption characteristics of a multilayered mushroom-type structure composed of thin material patches with a typical geometry as shown in Fig. 1. Aside from [17], in other previous work [10], [16], the vertical wires and patches have been assumed to be perfect electric conductors (PECs), and the present work concerns analysis of multilayer structure (shown in Fig. 1) with thin material (resistive) patches. Further, in [10] generalized additional boundary conditions (GABCs) have been derived for wire media terminated with distributed loads (metallic patch arrays acting as parallel loads to the wires) and lumped loads (arbitrary impedance insertions acting as series loads to the wires) or a combination of both at the junction, with the latter case presented in [47] and [48]. Although, the GABCs derived in [10] are applied at the wire-to-patch connection with the finite size of the patch (with certain restrictions imposed on the size of the gap between the patches with respect to the separation of adjacent patch arrays), these boundary conditions are valid only for perfect electric conductor terminations. However, the focus of the present paper is on the use of thin material interfaces at the wire medium connections (acting as parallel loads to the wires). Therefore, new ABCs (which generalize [17] to the multilayer case) have to be derived which take into account the finite conductivity of the material at the connection points.

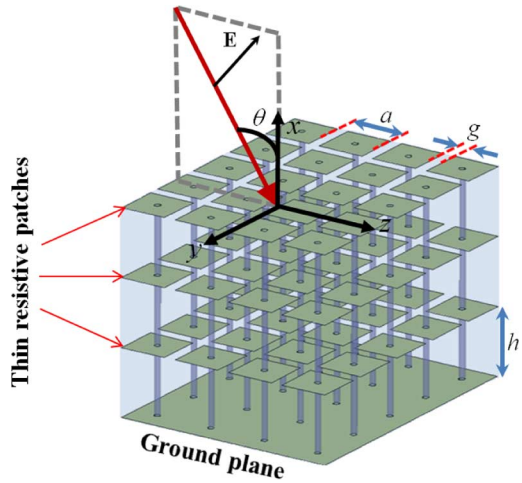

Fig. 1. Geometry of a multilayer mushroom structure formed by periodically loading a grounded wire medium with thin resistive patches.

To address this issue, in this paper we consider the case of wire media terminated with thin infinite resistive sheets or patch arrays (with $g \ll a$, where a is the period of the patches and the wires, and g is the gap between the adjacent patch elements), and derive ABCs at the connection of wires to a thin resistive sheet. The resulting ABCs are quite different than the previous ones for PEC patches. Based on these conditions, we then characterize the reflection properties of the multilayer mushroom-type structure (with a typical geometry shown in Fig. 1). The required ABCs for two-sided wire media with thin resistive sheets at the junction have not been presented previously, and is a new contribution of the paper. Further, we also aim to show that the presence of vias stabilizes the absorption response (as shown in [38] for a single-layer mushroom structure), enhances the absorption bandwidth (as shown in [39] for a single-layer mushroom structure), and increases the absorption performance for obliquely incident TM-polarized plane waves, making the multilayered mushroom structure an attractive candidate as an absorber.

It should be noted that although a simple transmission-line approach can be used to design some of the wideband absorbers (such as Jaumann, CA, and CCA), the analysis of the characteristics of a complicated structure such as the multilayer mushroom structure (considered in this work) using the transmission-line theory is not feasible. To overcome this drawback, in this paper we present a simple analytical model (based on homogenization of wire media with new ABCs at terminations) in order to model the reflection characteristics of the multilayer mushroom structure with thin material patches, and also a design guide for the analysis of wideband absorbers with stable angle characteristics. Moreover, the proposed model produces results almost instantaneously when compared to the full-wave numerical simulations carried out with the use of commercial programs such as HFSS [49].

The paper is organized as follows. In Section II, the ABCs are derived at the two-sided wire medium connection to a thin resistive sheet, and the formalism of the analytical model is presented for the analysis of the reflection characteristics of the multilayer mushroom-type structure. In Section III we validate the derived ABCs, and then present the results for the single-layer, two-layer, and three-layer mushroom structure absorbers. Finally in Section IV conclusions are drawn.

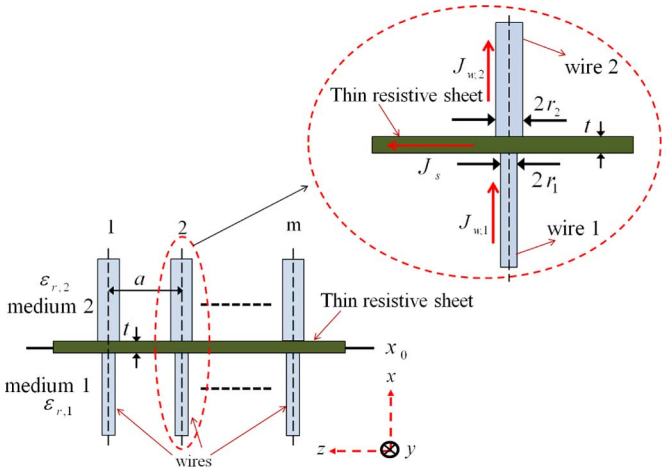

Fig. 2. Geometry of a junction of two wire mediums with a thin infinite resistive sheet at the interface.

II. Analytical Modelling of Multilayered Mushroom-Type HIS Absorbers

In this section, we present an analytical model for the reflection characteristics of a multilayered mushroom structure. The multilayer structure is formed by a stack of 2-D subwavelength thin conductive/resistive square patch FSS elements separated by dielectric slabs perforated with metallic pins (vias) and backed by a ground plane (with the geometry shown in Fig. 1). First, ABCs based on conservation of charge will be derived at the interface of two uniaxial wire mediums with a thin infinite imperfect conductor at the junction. Based on these conditions, the scattering problem of the multilayer structure for a patch array will then be solved for an obliquely incident TM-polarized plane wave, assuming that the gap between the patch elements is small compared to the period ($g \ll a$). The case of TE polarization is not of interest here, because the electric field is orthogonal to thin metallic vias and the interaction is negligible. In the following, a time variation of the form $e^{j\omega t}$ is assumed and suppressed.

A. Additional Boundary Conditions for a Double-Sided Wire Junction at Wire-to-Sheet Interface

Let us consider a junction between two uniaxial wire mediums with a thin infinite resistive sheet placed at the interface $x = x_0$ with the lattice period a (as shown in Fig. 2). In general, the sheet at the junction can be an arbitrary 2-D material such as graphene or a 2-D plasma characterized by a complex surface conductivity. It is assumed that the wires have different radii (r_1 and r_2) with $r_{1,2} \ll a$, and are embedded in dielectric host media with relative permittivities $\varepsilon_{r,1}$ and $\varepsilon_{r,2}$, respectively. Both the sheet and the difference in the wire media properties (i.e., wire radii and host permittivities) introduce irregularities in the charge and the current distributions close to the junction. We note, however, that the charge/current non-uniformity that arises due to the different wire radii can be neglected when $r_{1,2} \ll a$, which is the case considered here. For simplicity, we assume that the wires are lossless (PEC).

Consider a plane wave incident on the configuration shown in Fig. 2. In what follows, the term *microscopic* refers to currents and fields in the microstructure of the medium, i.e., on the wires and sheets of the actual physical structure. The term *macroscopic* refers to fields averaged over the lattice period, i.e., the fields in the equivalent homogenized (continuous) medium. Let $J_{w,1}$ and $J_{w,2}$ be the microscopic current densities induced on the surface of the wires in mediums 1 and 2 (with radii r_1 and r_2, respectively). Let σ_{2D} be the complex *surface* conductivity of the thin resistive sheet (such as graphene sheet with the surface conductivity given in [50]) placed at the interface. For thin materials with *bulk* conductivity σ_{3D}, the surface conductivity can be written as $\sigma_{2D} = \sigma_{3D} t$, where $t \ll \delta$ is the material thickness and $\delta = \sqrt{2/\omega\mu_0\sigma_{3D}}$ is the skin depth. On the thin conductive sheet, assumed local and isotropic, the microscopic current and the field are related as $J_s(y,z) = \sigma_{2D} E_t$, where J_s is the surface current density and E_t is the tangential electric field on the sheet. It should be noted that the tangential fields on the sheet in mediums 1 and 2 are assumed to be continuous at $x = x_0$, i.e.,

$$E_{t1}(x_0^-) = E_{t2}(x_0^+) = E_t. \tag{1}$$

The surface charge densities ρ_{s1} and ρ_{s2} on the PEC wires with radii r_1 and r_2 are given by $\rho_{s1}(x) = \varepsilon_0\varepsilon_{r,1}E_{n1}(x)$ and $\rho_{s2}(x) = \varepsilon_0\varepsilon_{r,2}E_{n2}(x)$, where E_{n1} and E_{n2} are the normal components of the microscopic electric fields at the wire surfaces. Considering that, at the wire-to-sheet and sheet-to-wire connection points (x_0^+ and x_0^-), the electric fields normal to the wires are the same as the tangential fields on the thin resistive sheet, we can write

$$E_{n1}(x_0^-) = E_{t1}(x_0^-) = \frac{\rho_{s1}(x_0^-)}{\varepsilon_0\varepsilon_{r,1}} \tag{2}$$

$$E_{n2}(x_0^+) = E_{t2}(x_0^+) = \frac{\rho_{s2}(x_0^+)}{\varepsilon_0\varepsilon_{r,2}}. \tag{3}$$

In addition, we have the continuity equation for the wires $\rho_{si} = -(1/j\omega)dJ_{w,i}(x)/dx$ ($i = 1, 2$). At the connection points (x_0^+ and x_0^-), the surface charge densities can be written as

$$\rho_{s1}(x_0^-) = -\frac{1}{j\omega}\frac{dJ_{w,1}(x)}{dx}\Big|_{x_0^-} \tag{4}$$

$$\rho_{s2}(x_0^+) = -\frac{1}{j\omega}\frac{dJ_{w,2}(x)}{dx}\Big|_{x_0^+}. \tag{5}$$

From Fig. 2, using Kirchoff's current law (conservation of charge) at the junction of two wire mediums with thin resistive sheet at the interface, we have

$$J_s = J_{w,1} - J_{w,2}. \tag{6}$$

Using (1), the surface current density can be expressed as

$$J_s = \sigma_{2D}E_t = \sigma_{2D}E_{t1}(x_0^-) = \sigma_{2D}E_{t2}(x_0^+) = \sigma_{2D}\frac{\left[E_{t1}(x_0^-) + E_{t2}(x_0^+)\right]}{2}. \tag{7}$$

Equating now (6) and (7) and using (4) and (5) in the expression for the tangential fields (2) and (3) we obtain the following ABC:

$$\frac{\sigma_{2D}}{2j\omega\varepsilon_0}\left[\frac{1}{\varepsilon_{r,1}}\frac{dJ_{w,1}(x)}{dx}\Big|_{x_0^-} + \frac{1}{\varepsilon_{r,2}}\frac{dJ_{w,2}(x)}{dx}\Big|_{x_0^+}\right] + \left[J_{w,1}(x_0^-) - J_{w,2}(x_0^+)\right] = 0. \tag{8}$$

By enforcing the continuity of tangential fields at the thin conductive sheet interface (1), we obtain the second ABC for the microscopic wire current:

$$\frac{1}{\varepsilon_{r,1}}\frac{dJ_{w,1}(x)}{dx}\bigg|_{x_0^-} - \frac{1}{\varepsilon_{r,2}}\frac{dJ_{w,2}(x)}{dx}\bigg|_{x_0^+} = 0. \tag{9}$$

In Section II-B, it will be shown that the ABCs (8) and (9) are essential in solving the reflection problem of a multilayered mushroom structure. Also, it is worth noting that the conditions (8) and (9) derived in this section are applicable to the cases of different conductivities of the thin conductive patch at the wire-medium junction, provided the gap between the patch elements is much smaller than the period $g \ll a$.

For the limiting case of the identical wire media on either side of the thin resistive sheet interface at x_0 (i.e., $\varepsilon_{r,1} = \varepsilon_{r,2} = \varepsilon_r$ and $r_1 = r_2 = r$), the ABCs (8) and (9) in this case can be obtained by enforcing the continuity of surface charge densities and using the Kirchoff's current law at the connection points x_0^+ and x_0^-, i.e., $\rho_{s1}(x_0^-) = \rho_{s2}(x_0^+) = \rho_s = \varepsilon_0\varepsilon_r J_s/\sigma_{2D} = (\rho_{s1}(x_0^-) + \rho_{s2}(x_0^+))/2$ and $J_w(x_0^-) = J_s + J_w(x_0^+)$.

In the limiting case of $\sigma_{2D} \to 0$, (transparent sheet) we have a continuous wire-medium slab with simple continuity conditions for the current: $J_w(x_0^+) = J_w(x_0^-)$ and $dJ_w(x)/dx|_{x_0^+} = dJ_w(x)/dx|_{x_0^-}$. For $\sigma_{2D} \to \infty$, we have a perfect electric conducting ground plane with the ABC for wire microscopic currents given by $dJ_w(x)/dx|_{x_0^+} = dJ_w(x)/dx|_{x_0^-} = 0$, i.e., the derivative of each of the wire currents is independently zero at the connection points. This result is consistent with the result of the single-sided wire-medium junction with a conducting ground plane [8]. In addition, with the assumption that $g \ll a$, the above result has been successfully used for characterizing various mushroom-type structures, which include a single-layer mushroom structure terminated with PEC patches [14], [15] and a multilayer mushroom structure [16] for characterizing negative refraction. However, for moderate and large gaps between the patches these boundary conditions give inaccurate results. To overcome this issue GABCs similar to those proposed in [10] (for the PEC patches) have to be considered

$$\frac{dJ_w(x)}{dx}\bigg|_{x_0^+} + \frac{dJ_w(x)}{dx}\bigg|_{x_0^-} = \frac{2C}{C_0}\left[J_w(x_0^+) - J_w(x_0^-)\right] \tag{10}$$

$$\frac{dJ_w(x)}{dx}\bigg|_{x_0^+} - \frac{dJ_w(x)}{dx}\bigg|_{x_0^-} = 0 \tag{11}$$

where C is the capacitance of the wires and C_0 is the capacitance of the metallic patch which depends on the period a and gap g (the values of C and C_0 are defined in [10]). These ABCs are accurate for moderate and large gaps between the patches, provided the distance h between the metallic patches in adjacent layers is much greater than g. When the gap between the patches reduces and $C_0 \to \infty$, we have a perfect electric conducting ground plane with the ABCs (10) and (11) reduce to $dJ_w(x)/dx|_{x_0^+} = dJ_w(x)/dx|_{x_0^-} = 0$, which is the same expression obtained above from (8), (9) when $\sigma_{2D} \to \infty$. However, the GABCs (10) and (11) apply to the modeling of wire media with metallic (PEC) terminations, whereas the ABCs (8), (9) obtained in this paper deal with thin material (resistive) terminations (however, gap capacitance is not accounted for).

Further, it is interesting to note that the ABCs (8) and (9) derived in this section for the double-sided wire medium are generalizations of the simpler (single-sided) case studied in [17], i.e., one can obtain the ABC given in [17] by letting either $J_{w,1} = 0$ or $J_{w,2} = 0$. For example, for the case of wires in the half-space $x < x_0$, the ABC reads

$$J_{w,1}(x_0^-) + \frac{\sigma_{2D}}{j\omega\varepsilon_0\varepsilon_{r,1}}\frac{dJ_{w,1}(x)}{dx}\bigg|_{x_0^-} = 0 \tag{12}$$

which corresponds exactly to the ABC derived in [17, eq. (5)]. Therefore, while a single ABC is sufficient to describe the electromagnetic phenomenon of a single-sided wire-medium junction, the general case of a double-sided junction requires two ABCs, and the fact that the termination is resistive rather than metallic leads to the new ABCs presented in this paper. In relation to the ABCs (8) and (9), below we summarize some of the ABCs developed in literature for terminated wire media. In [14]–[16], the ABCs are valid for single-sided and double-sided wire media terminated with PEC patches, which do not take into account the gap capacitance, i.e., are valid only for $g \ll a$. In [10], the ABCs are valid for wire media terminated with PEC patches for moderate and large gaps between the patches, i.e., takes into account the gap capacitance. In [17], the ABCs are derived for single-sided wire media terminated by thin resistive sheets and are applicable to resistive patches, provided $g \ll a$, i.e., does not take into account the gap capacitance.

B. Scattering Problem of the Multilayered Mushroom-Type Absorber

In order to illustrate the application of the new ABCs (8) and (9), here we study the scattering problem of a multilayered mushroom structure with the geometry as that shown in Fig. 3 (a is the period of the patches and vias). It is assumed that each dielectric layer, perforated with thin metallic vias of radius $r_l \ll a$, is homogeneous and isotropic of thickness h_l, characterized by relative permittivity $\varepsilon_{r,l}$ and permeability of free space, and loaded with 2-D periodic thin conductive patches of conductivity $\sigma_{2D,l}$ at the interface d_l, $l = 1, 2, \ldots, m$. The objective is to obtain the reflection characteristics of the structure for a TM plane-wave incidence. It should be noted that the ABCs (8) and (9) derived in Section II-A are applicable to resistive patch arrays when the gap between the patch elements is much smaller than the period ($g \ll a$) since they are derived for an infinite sheet.

Consider a time-harmonic plane wave incident on the multilayer mushroom structure shown in Fig. 3. Each wire-medium slab is characterized by the nonlocal dielectric function [5], [7] $\varepsilon_{\text{eff},l} = \varepsilon_0\varepsilon_{r,l}\left[\varepsilon_{xx,l}(\omega, k_x)\hat{x}\hat{x} + \hat{y}\hat{y} + \hat{z}\hat{z}\right]$, where $\varepsilon_{xx,l}(\omega, k_x) = 1 - k_{p,l}^2/(k_{h,l}^2 - k_x^2)$, $k_{h,l} = k_0\sqrt{\varepsilon_{r,l}}$ is the wavenumber in the host material, k_0 is the wavenumber in free space, $k_{p,l}$ is the plasma wavenumber which depends on the period and radius of the vias: $k_{p,l}^2 = (2\pi/a^2)/[\ln(a/2\pi r_l) + 0.5275]$, and k_x is the x-component of the wave vector $\mathbf{k} = (k_x, 0, k_z)$. Let $J_{w,l}$ be the surface current densities induced on the metallic wires. It is known that for a TM plane-wave incidence, the wire medium excites both transverse electromagnetic (TEM) and TM^x modes, and thus,

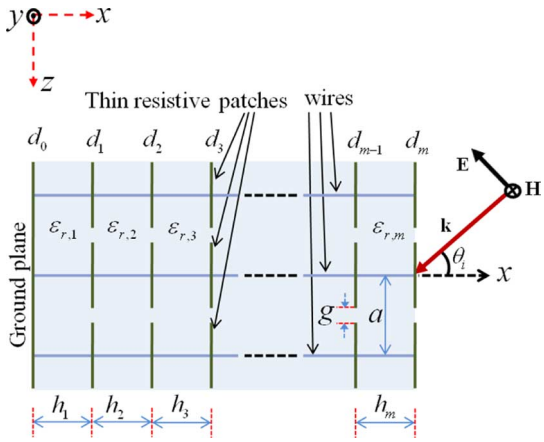

Fig. 3. Schematic of a generic multilayer mushroom structure formed by periodically loading grounded wire medium with thin resistive square patches (side view).

following [7], the electric and magnetic fields in the air region $(x > d_m)$ are given by

$$\eta_0 H_y = e^{\gamma_0 (x-d_m)} + Re^{-\gamma_0 (x-d_m)} \tag{13}$$

$$E_z = \frac{-j\gamma_0}{k_0}\left[e^{\gamma_0 (x-d_m)} - Re^{-\gamma_0 (x-d_m)}\right] \tag{14}$$

and the fields in the wire-medium slab $(d_{l-1} < x < d_l)$ can be written as

$$\eta_0 H_y^{(l)} = A^+_{\mathrm{TM},l} e^{\gamma_{\mathrm{TM},l}(x-d_{l-1})} + A^-_{\mathrm{TM},l} e^{-\gamma_{\mathrm{TM},l}(x-d_{l-1})} + B^+_{\mathrm{TEM},l} e^{\gamma_{\mathrm{TEM},l}(x-d_{l-1})} + B^-_{\mathrm{TEM},l} e^{-\gamma_{\mathrm{TEM},l}(x-d_{l-1})} \tag{15}$$

$$E_x^{(l)} = \frac{k_z}{\varepsilon^{\mathrm{TM}}_{xx,l} k_0 \varepsilon_{r,l}} \times \left[A^+_{\mathrm{TM},l} e^{\gamma_{\mathrm{TM},l}(x-d_{l-1})} + A^-_{\mathrm{TM},l} e^{-\gamma_{\mathrm{TM},l}(x-d_{l-1})}\right] \tag{16}$$

$$E_z^{(l)} = \frac{-j\gamma_{\mathrm{TM},l}}{\varepsilon_{r,l} k_0} \times \left[A^+_{\mathrm{TM},l} e^{\gamma_{\mathrm{TM},l}(x-d_{l-1})} - A^-_{\mathrm{TM},l} e^{-\gamma_{\mathrm{TM},l}(x-d_{l-1})}\right] - \frac{j\gamma_{\mathrm{TEM},l}}{\varepsilon_{r,l} k_0}\left[B^+_{\mathrm{TEM},l} e^{\gamma_{\mathrm{TEM},l}(x-d_{l-1})} - B^-_{\mathrm{TEM},l} e^{-\gamma_{\mathrm{TEM},l}(x-d_{l-1})}\right] \tag{17}$$

where $d_l = h_1 + h_2 + \cdots + h_l$, $l = 1, 2, \ldots, m$, $\eta_0 = \sqrt{\mu_0/\epsilon_0}$ is the free-space impedance, R is the reflection coefficient, $A^{\pm}_{\mathrm{TM},l}$, $B^{\pm}_{\mathrm{TEM},l}$ are the amplitude coefficients of the TM and TEM fields, $\gamma_0 = \sqrt{k_z^2 - k_0^2}$, $\varepsilon^{\mathrm{TM}}_{xx,l} = 1 - k_{p,l}^2/(k_z^2 + k_{p,l}^2)$, $\gamma_{\mathrm{TEM},l} = jk_0\sqrt{\epsilon_{r,l}}$, $\gamma_{\mathrm{TM},l} = \sqrt{k_{p,l}^2 + k_z^2 - k_{h,l}^2}$, and $k_z = k_0 \sin\theta_i$.

To calculate the unknown coefficients, R, $A^{\pm}_{\mathrm{TM},l} B^{\pm}_{\mathrm{TEM},l}$, we impose boundary conditions at $x = 0$, $d_1, d_2, \ldots, d_m$. Since, there are m dielectric layers and m interfaces, we have the total number of unknowns as $4m + 1$ (i.e., four unknowns in each layer corresponds to $4m$, and the remaining unknown is R). Hence, $4m + 1$ boundary conditions are necessary to calculate the $4m + 1$ unknown coefficients. At the thin resistive patch interfaces $(x = d_l^{\pm}, l = 1, \ldots, m)$, the macroscopic two-sided impedance boundary conditions establish that the tangential electric $(E_z^{(l)})$ and magnetic fields $(H_y^{(l)})$, can be related via a sheet impedance, i.e.,

$$E_z^{(l)}|_{x=d_l^+} = E_z^{(l)}|_{x=d_l^-} = Z_{g,l}\left(H_y^{(l+1)}|_{x=d_l^+} - H_y^{(l)}|_{x=d_l^-}\right) \tag{18}$$

where $Z_{g,l}$ is the grid impedance of the thin conductive patches [17], [51], [52] given by

$$Z_{g,l} = \frac{a}{(a-g)\sigma_{2D,l}} - j\frac{\pi}{2\omega\varepsilon_0(\varepsilon^{qs}_{r,l})a\ln\left(\csc\frac{\pi g}{2a}\right)} \tag{19}$$

where $\varepsilon^{qs}_{r,l} = (\varepsilon_{r,l} + \varepsilon_{r,l+1})/2$ for interior patches $(l = 1, 2, \ldots, m-1)$ and $\varepsilon^{qs}_{r,m} = (\varepsilon_{r,m} + 1)/2$ for the patch located at the upper interface $(l = m)$. This gives $2m$ boundary conditions. At the ground plane interface $(x = 0^+)$, we have two more boundary conditions [7]: i) tangential macroscopic total electric field vanishes $(E_z^{(1)}|_{x=0^+} = 0)$ and ii) derivative of current is zero $(dJ_{w,1}(x)/dx|_{x=0^+} = 0)$, [8], or in terms of macroscopic fields,

$$\left[k_0\varepsilon_{r,1}\frac{dE_x^{(1)}(x)}{dx} - k_z\eta_0\frac{dH_y^{(1)}(x)}{dx}\right]_{x=0^+} = 0. \tag{20}$$

Following [17], the boundary condition at the top patch interface, $x = d_m^-$, can be written as

$$J_{w,m}(d_m^-) + \frac{\sigma_{2D,m}}{j\omega\varepsilon_0\varepsilon_{r,m}}\frac{dJ_{w,m}(x)}{dx}\bigg|_{d_m^-} = 0 \tag{21}$$

or, equivalently, the following macroscopic field condition:

$$\left(1 + \frac{\sigma_{2D,m}}{j\omega\varepsilon_0}\frac{d}{dx}\right)\left[k_0 E_x^m(x) - \frac{k_z\eta_0}{\varepsilon_{r,m}}H_y^m(x)\right]_{d_m^-} = 0. \tag{22}$$

This gives the total number of $2m + 3$ conditions, clearly insufficient to calculate the $4m + 1$ unknown coefficients, which makes apparent the need of the ABCs derived in Section II-A.

At the junction of two wire mediums with thin conductive patches at the interfaces $(x = d_l^{\pm}, l = 1, \ldots, m-1)$ it is necessary to impose the ABCs (8) and (9), in addition to the boundary condition (18)

$$\frac{\sigma_{2D,l}}{2j\omega\varepsilon_0}\left[\frac{1}{\varepsilon_{r,l}}\frac{dJ_{w,l}(x)}{dx}\bigg|_{d_l^-} + \frac{1}{\varepsilon_{r,l+1}}\frac{dJ_{w,l+1}(x)}{dx}\bigg|_{d_l^+}\right] + \left[J_{w,l}(d_l^-) - J_{w,l+1}(d_l^+)\right] = 0 \tag{23}$$

$$\frac{1}{\varepsilon_{r,l}}\frac{dJ_{w,l}(x)}{dx}\bigg|_{d_l^-} - \frac{1}{\varepsilon_{r,l+1}}\frac{dJ_{w,l+1}(x)}{dx}\bigg|_{d_l^+} = 0. \tag{24}$$

In terms of macroscopic fields, (23) and (24) can be rewritten as

$$\left(1 + \frac{\sigma_{2D,l}}{2j\omega\varepsilon_0}\frac{d}{dx}\right)\left[k_0 E_x^{(l)}(x) - \frac{k_z\eta_0}{\varepsilon_{r,l}}H_y^{(l)}(x)\right]_{d_l^-} = \left(1 - \frac{\sigma_{2D,l}}{2j\omega\varepsilon_0}\frac{d}{dx}\right) \times \left[k_0 E_x^{(l+1)}(x) - \frac{k_z\eta_0}{\varepsilon_{r,l+1}}H_y^{(l+1)}(x)\right]_{d_l^+} \tag{25}$$

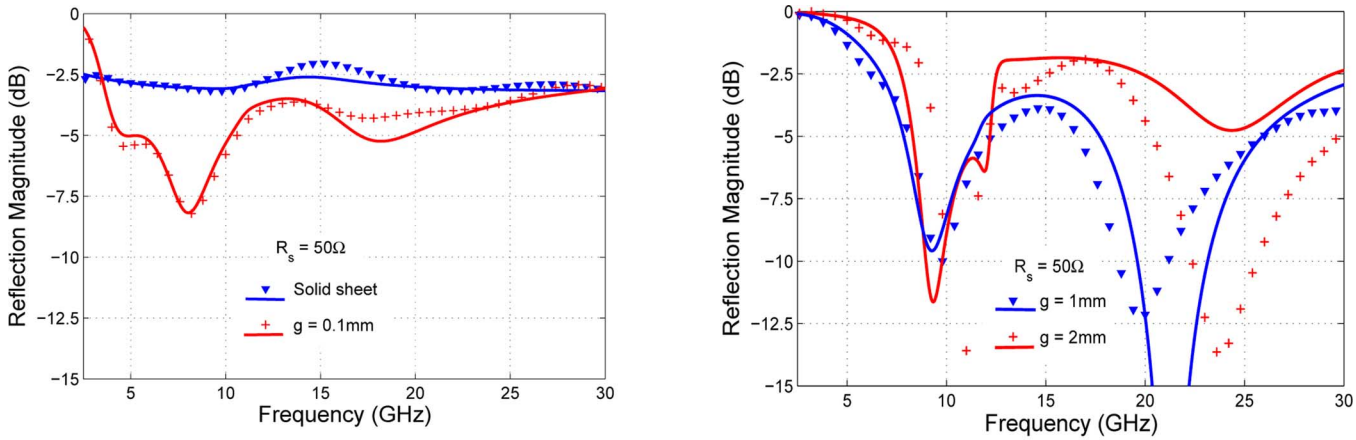

(a) (b)

Fig. 4. Comparison of analytical (solid lines) and full-wave HFSS results (symbols) of the reflection coefficient for the two-layer mushroom HIS absorber (with geometry and parameters shown in Fig. 13) with $R_{s1} = R_{s2} = 50\ \Omega$, $\theta = 45^\circ$: (a) solid sheet and $g_1 = g_2 = 0.1$ mm and (b) $g_1 = g_2 = 1$ mm and $g_1 = g_2 = 2$ mm.

$$\frac{d}{dx}\left[k_0 E_x^{(l)}(x) - \frac{k_z \eta_0}{\varepsilon_{r,l}} H_y^{(l)}(x)\right]_{d_l^-} = \frac{d}{dx}\left[k_0 E_x^{(l+1)}(x) - \frac{k_z \eta_0}{\varepsilon_{r,l+1}} H_y^{(l+1)}(x)\right]_{d_l^+}. \quad (26)$$

Since there are $m-1$ layers of two-sided wire-medium junctions, we have $2(m-1)$ boundary conditions and hence, the total number of boundary conditions are equal to $4m+1$. Using the boundary conditions (18), (20), (22), (25) and (26), we can easily obtain a linear system for the $4m+1$ unknowns of the problem. This system can be solved either numerically or analytically for the unknown field coefficients, $A^{\pm}_{\mathrm{TM},l}$ and $B^{\pm}_{\mathrm{TEM},l}$, and the reflection coefficient R.

III. Numerical Results and Discussions

In this section, we first validate the proposed ABCs for the junction of two-wire media separated by thin resistive patch arrays by comparing the analytical model results with the full-wave numerical simulations. Then we study wideband absorption characteristics of single-layer, two-layer, and three-layer mushroom structures (with the geometries shown in Figs. 7, 13, and 18, respectively) for obliquely incident TM-polarized plane waves. More remarkably, by employing the proposed structure, we show that vias can be used to increase the bandwidth and enhance absorptivity for the TM-polarized oblique incidence, by utilizing the resonances of the mushroom and wire-medium HIS structures. The results obtained using the analytical model for all the three structures are confirmed with lengthy full-wave numerical simulations.

A. Validity of the Analytical Model

Since the ABCs proposed in this work are derived for the interface of the wire media separated by a thin infinite (continuous) resistive sheet at the junction, they have to be thoroughly verified while applying to the resistive patch connections, wherein the gap g between the patches plays an important role. To understand the effect of g on the applicability of the proposed ABCs, here we consider a two-layer mushroom structure (with the geometry and parameters given in Fig. 13), and study its reflection magnitude behavior for varying resistivity R_s and g of the resistive patch arrays using the analytical model given in Section II. Here R_s is the sheet resistance, which depends on the bulk conductivity $\sigma_{3D}(\mathrm{S/m})$ of the material, i.e., $R_s = 1/\sigma_{2D} = 1/(\sigma_{3D} t)$. From (19) one can represent the grid impedance of the lossy patch array as a series RC circuit $(R_g - j/(\omega C_g))$, where the real value corresponds to R_g (resistance per unit cell) given by $a/((a-g)\sigma_{2D})$ or $R_s a/(a-g)$ and the imaginary value corresponds to $-1/(\omega C_g)$ (capacitive impedance) whose value can be obtained from (19). We first consider the case of oblique incidence $\theta = 45^\circ$, with a low value of resistivity fixed in both the layers, i.e., $R_{s1} = R_{s2} = R_s = 50\ \Omega$ and study the reflection magnitude behavior versus frequency for increasing values of g. It is assumed here that g takes the same value in both the patch array layers $(g_1 = g_2 = g)$. The results are shown in Fig. 4(a) and (b). It is clear that, for solid sheet and for $g = 0.1$ mm [Fig. 4(a)], the analytical model results are in good agreement with the full-wave simulation results. However, as g increases (i.e., for 1 mm and 2 mm cases), one can notice the discrepancies between the analytical model and numerical simulation results [Fig. 4(b)]. This is due to the fact that the capacitive impedance (i.e., the imaginary part of the grid impedance expression) of the patch array dominates the resistivity of the patches, and since the ABCs (8) and (9) derived in this work do not take into account the capacitance of the patches for large gaps, the analytical model results are not accurate. In the next scenario, we choose a high value of resistivity for the patch arrays in both the layers, and study a similar behavior as that shown in Fig. 4. The results are plotted in Fig. 5 for various values of g. It can be noticed that as g increases, the reflection magnitude behavior calculated using the analytical model agrees well with the numerical results, even for large values of g (e.g., for $g = 2$ mm). In fact, for the same mushroom structure considered above with the PEC patches, with period a and gap g comparable to the separation h between the patch arrays in the adjacent layers, the ABCs (10) and (11) may give inaccurate results. However, (10) and (11) give accurate results provided $h \gg g$. Surprisingly, the ABCs (8) and (9) obtained in this work are valid even when g is large and comparable to h,

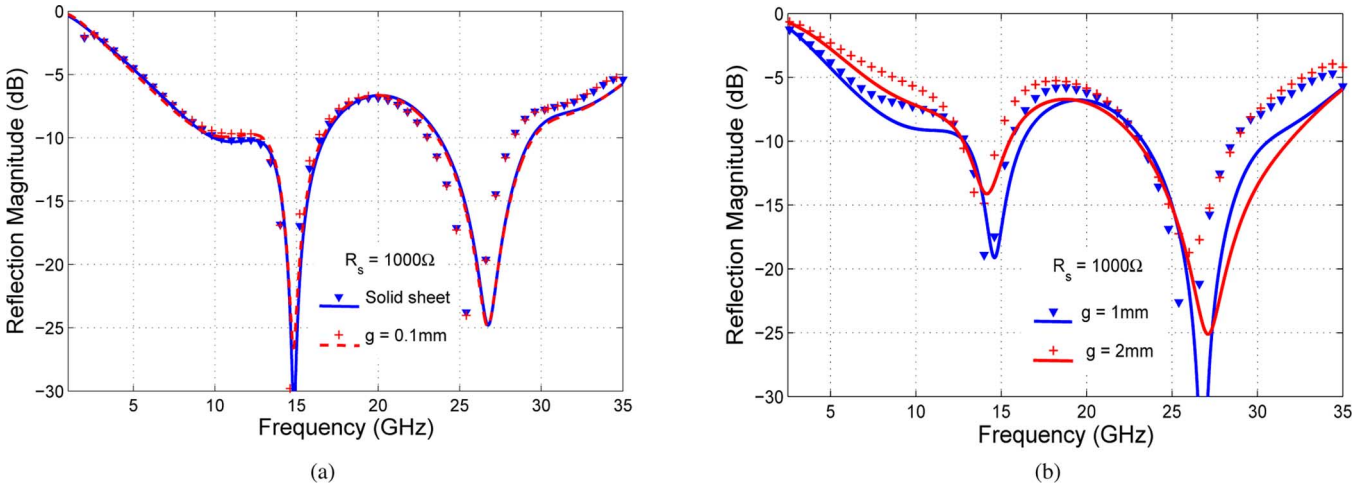

Fig. 5. Comparison of analytical (solid lines) and full-wave HFSS results (symbols) of the reflection coefficient for the two-layer mushroom HIS absorber (with geometry and parameters shown in Fig. 13) with $R_{s1} = R_{s2} = 1000\ \Omega$, $\theta = 45°$: (a) solid sheet and $g_1 = g_2 = 0.1$ mm and (b) $g_1 = g_2 = 1$ mm and $g_1 = g_2 = 2$ mm.

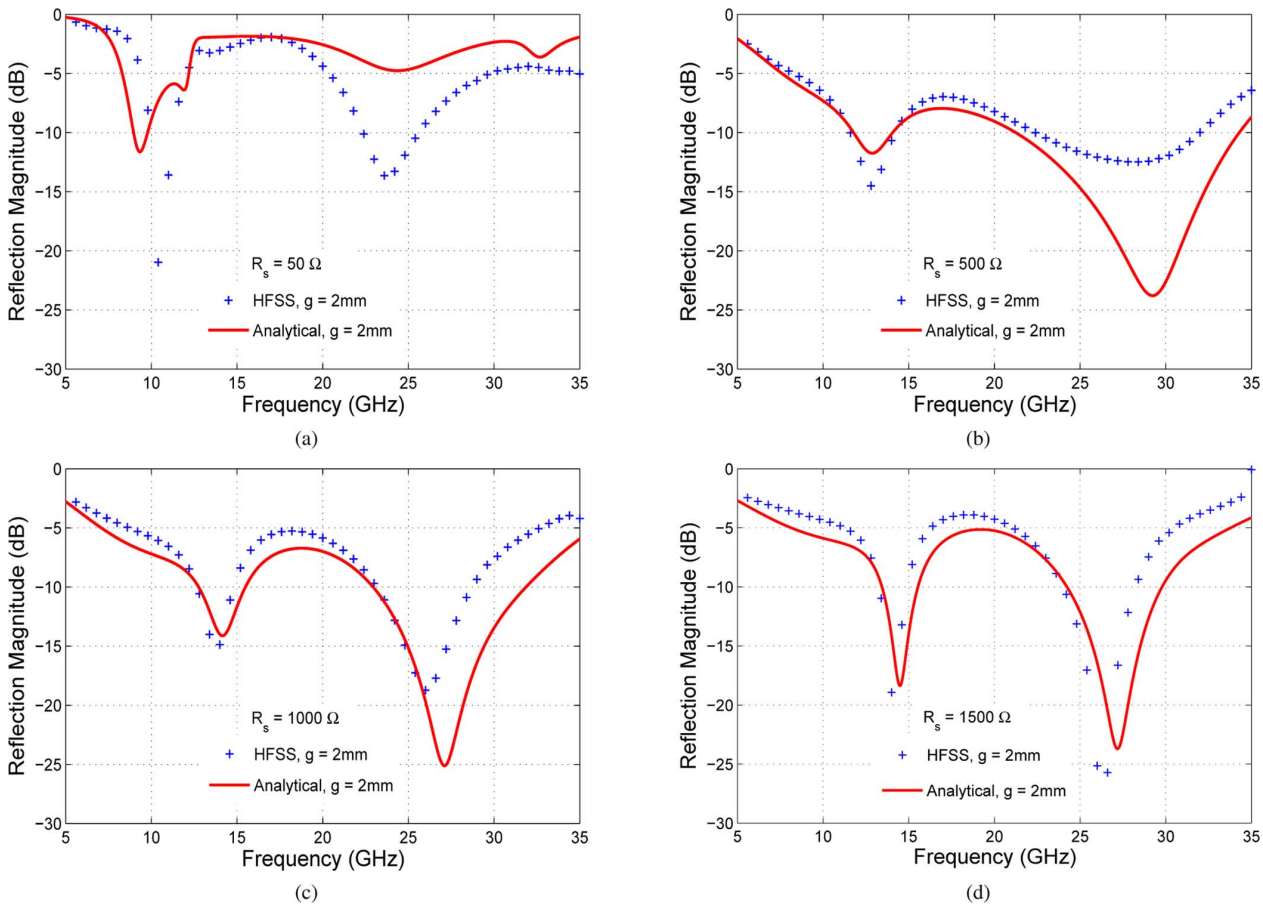

Fig. 6. Comparison of analytical (solid lines) and full-wave HFSS results (symbols) of the reflection coefficient for the two-layer mushroom HIS absorber (with geometry and parameters shown in Fig. 13) for different resistivities of the patch arrays with $g_1 = g_2 = 2$ mm, $\theta = 45°$: (a) $R_{s1} = R_{s2} = 50\ \Omega$, (b) $R_{s1} = R_{s2} = 500\ \Omega$, (c) $R_{s1} = R_{s2} = 1000\ \Omega$, and (d) $R_{s1} = R_{s2} = 1500\ \Omega$.

though the conditions are derived for solid resistive sheets. This is due to the fact that the resistivity of the patch arrays dominates over the capacitive impedance. Further, it can be noticed from Fig. 5 that the reflection magnitude behavior does not show much variations for increasing values of g. This is again due to the fact that the value of capacitive impedance of the patch arrays with large gaps (even though it is large when compared to patch arrays with small gaps) is small when compared to the resistivity. In such a case, one can approximate the behavior of these patch arrays using a solid sheet of large resistivity.

To further clarify the effect of resistivity, in Fig. 6 we show the variation of reflection magnitude behavior versus frequency for different values of the sheet resistivities of the patch arrays of a similar structure studied in Figs. 4 and 5, however, for a fixed large gap value, i.e., for $g_1 = g_2 = g = 2$ mm. It can be noticed that with an increase in the sheet resistivity of the patch

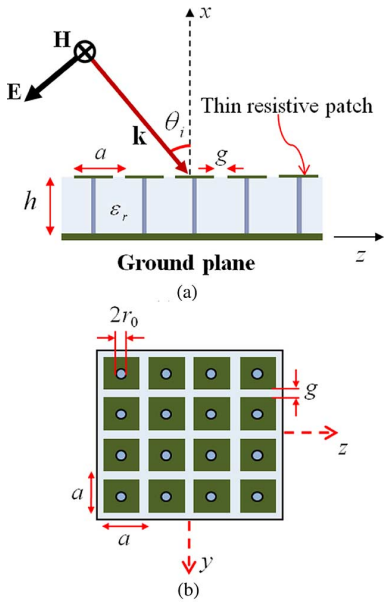

Fig. 7. (a) Single-layer mushroom-type HIS absorber with thin resistive patches. (b) Top view of the structure.

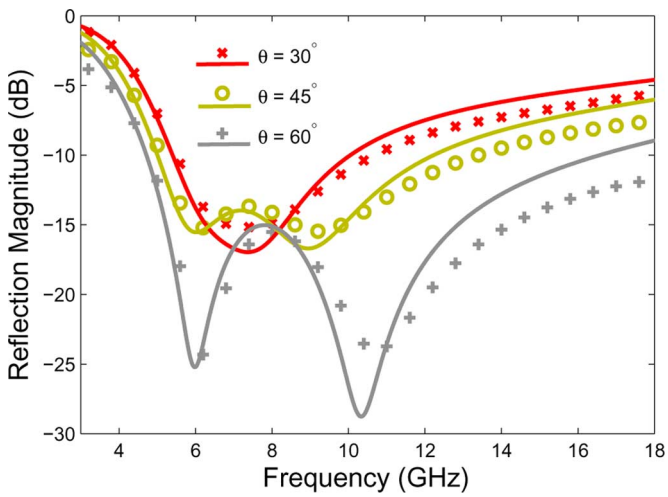

Fig. 8. Comparison of analytical (solid lines) and full-wave HFSS results (crosses, circles, and plus signs) of the reflection coefficient for the single-layer mushroom HIS absorber excited by a TM-polarized plane wave at oblique angles of incidence θ.

arrays, the analytical model results start to agree with the numerical simulation results. This clearly demonstrates that when the resistivity of patch arrays is dominant over the capacitive impedance, the proposed ABCs give accurate results.

Thus, it is clear from the above analysis that for large gaps, as long as the capacitive impedance is less dominant than the resistivity of the patch arrays, the ABCs derived for the wire-sheet-wire connections can be accurately used to model wire-patch-wire junctions [for example, $R_s = 1000\ \Omega$ and $g = 2$ mm, as shown in Fig. 5(b)], however, for small gaps, the ABCs derived are valid for any resistivity of the patch arrays [for example, $R_s = 50\ \Omega$ and $g = 0.1$ mm, as shown in Fig. 4(a), and $R_s = 1000\ \Omega$ and $g = 0.1$ mm, as shown in Fig. 5(a)]. Further, in the case of patch arrays with very small gaps, the behavior could be well approximated using a solid sheet even if sheet resistivity is low or high (and still large enough to dominate the

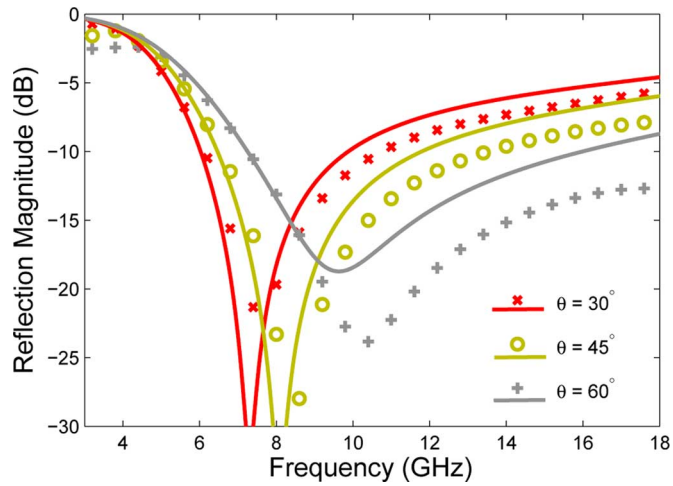

Fig. 9. Comparison of analytical (solid lines) and full-wave HFSS results (crosses, circles, and plus signs) of the reflection coefficient for the single-layer HIS absorber (without vias) excited by a TM-polarized plane wave at oblique angles of incidence θ.

reactive part of the impedance), however, for patch arrays with large gaps, the replacement of the patch array by a solid sheet is only valid when the sheet resistivity is sufficiently large.

B. Single-Layer Mushroom Structure With Thin Resistive Patches

To demonstrate the performance of the proposed absorber (the multilayered mushroom structure shown in Fig. 1), we begin with the analysis of the reflection properties of the single-layer mushroom structure shown in Fig. 7 composed of an array of thin resistive patches printed over a grounded dielectric slab perforated with metallic vias.

Although this structure is similar to the one studied in [17], we employ this example to show that the mushroom structure (with resistive patches), when designed properly, enhances the absorption bandwidth for increasing angles of the obliquely incident TM-polarized plane wave. To show this effect, we consider the following parameters in the design of the absorber: $a = 6.8$ mm, $g = 0.5$ mm, $h = 3.5$ mm, $r_0 = 0.08$ mm, $\varepsilon_r = 2.5$, and $R_s = 106.54\ \Omega$. The rationale behind the choice of this particular value of R_s will be discussed later in this section. Fig. 8 shows the reflection coefficient for the incident angles of 30°, 45°, and 60°. The results obtained using the analytical model described in Section II (for the limiting case of single-sided wire-to-patch junction), and in [17], agree well with the full-wave HFSS results. In order to demonstrate the advantage of the mushroom-type absorber, in Fig. 9 we present the behavior of the reflection coefficient for a similar structure without vias, with the parameters listed above. In the absence of vias, the absorber can be easily modeled using a simple circuit theory model given in [52]–[54]. Again, the results obtained using the circuit model are in good agreement with the HFSS results. It is observed that for large angles of incidence, the absorption bandwidth is increased in Fig. 8 as compared to the case of the same structure without the vias (Fig. 9). In Fig. 8 it is noticed that the lower frequency bound of the absorption band (around 6 GHz) is stable, which is in complete contrast to the behavior of the structure without vias (Fig. 9). This frequency

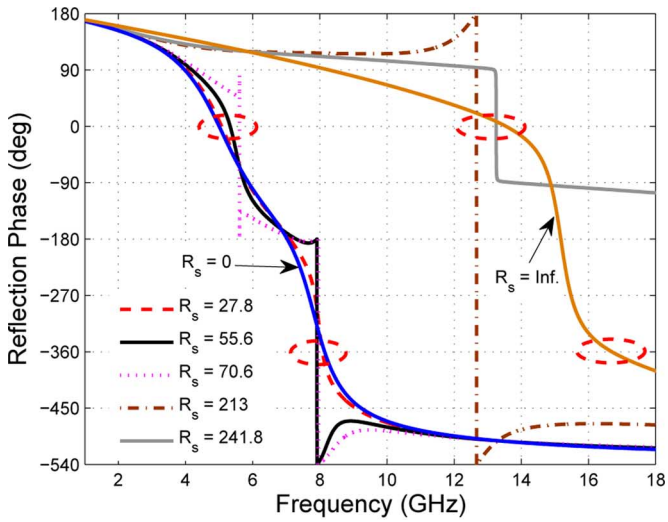

(a)

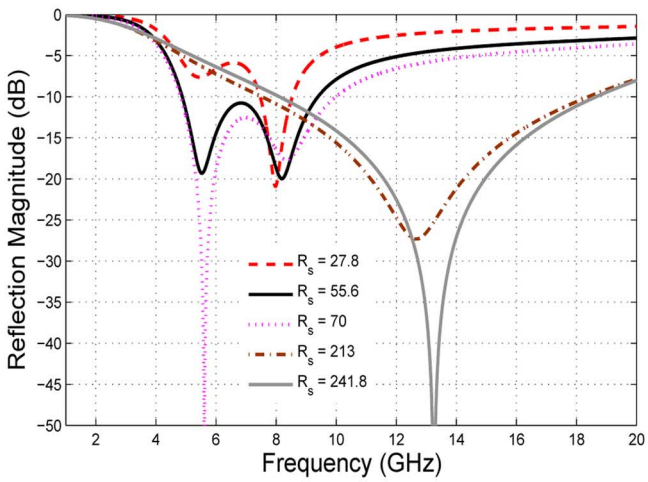

(b)

Fig. 10. (a) Phase and (b) magnitude of the reflection coefficient of the single-layer mushroom structure for different values of sheet resistivity R_s (in Ω), $\theta = 45°$.

stability can be attributed to the increased interaction of the incident wave with the vias. Furthermore, it is shown in Fig. 8 that the enlargement of the absorption band allows to maintain good absorption at the center frequency of the band for different angles of incidence, providing better performance with respect to the structure without vias.

To understand the physical reasons of the wideband absorption in the mushroom structure, in Fig. 10, we show the reflection properties (phase and magnitude) for a TM-polarized plane wave incident at 45°, for different resistive values (for R_s ranging from 0 to ∞; i.e., from the PEC patch to the transparent patch) of the thin resistive patch arrays using the analytical model. Starting with the PEC patch case (i.e., $R_s = 0$ or $\sigma_{3D}t = \infty$), the reflection phase behavior shows two resonances [shown in red circles in Fig. 10(a)] corresponding to the 0° or 360° phase (acting as a HIS), consistent with the result of the HIS discussed in [14], [15]. These resonances are such that one lies above the plasma frequency ($f_p/\sqrt{\varepsilon}_r = 6.28$ GHz) and the other lies below $f_p/\sqrt{\varepsilon}_r$. However, this is not the case for the structure without vias, where there is only one HIS resonance. The additional resonance of the mushroom structure, along with the proper choice of resistivity of the patch arrays and the fact that obliquely incident TM-polarized plane waves interact strongly with the vias, will be used to design wideband absorbers with enhanced absorption. With the increase in the resistive sheet values, one can notice in Fig. 10(a) the deviation of the reflection phase behavior from the actual HIS performance. The reason for this behavior is quite simple: a change in the sheet resistivity values affects the grid impedance [see (19)] of the patch array, which further changes the surface impedance of the mushroom structure. This deviation of the reflection phase behavior (resonances) is referred to as perturbed HIS behavior. Also, increasing the resistivity of the patch arrays increases the losses in the structure. As a result, a fraction of the total energy of the incident wave will be absorbed, depending on the values of the sheet resistivity [shown in Fig. 10(b)]. For example, a value of sheet resistivity of $R_s = 27.8\ \Omega$, whose reflection magnitude behavior shows two reflection minima [dashed red curve in Fig. 10(b)], corresponds closely to the two perturbed HIS resonances [Fig. 10(a)].

By slowly increasing the sheet resistivity, there is a shift in the absorption levels of the two reflection minima (i.e., one of the reflection minima deepens, and the other minima either subdues or remains the same). This is due to match/mismatch of the surface impedance of the structure to the free-space impedance at those frequencies. In particular, for the sheet resistivity values of 70.6 Ω and 241.8 Ω, we have perfect absorption for one of the reflection minima (at frequencies 5.612 GHz and 13.25 GHz, respectively). Under this condition the zero reflection phases shown in Fig. 10(a) correspond exactly to these frequencies. This proves the fact that the reflection minima shown in Fig. 8, for the case of $R_s = 106.54\ \Omega$ are nothing but the perturbed HIS resonances of the actual HIS structure with PEC patches. Hence, by utilizing the two resonances of the mushroom structure, along with the proper choice of resistivity of patch arrays, the absorption bandwidth is enlarged. This is not noticed in the structure without vias, where a single resonance of the HIS exists, and hence, the absoption band is narrow. With further increase in the resistivity of the patch arrays (as $R_s \to \infty$ $[\sigma_{3D}t \to 0]$ the patch array is fully transparent), we reach the case of the wire-medium slab (bed-of-nails) [15], which shows two resonances corresponding to zero phase (acting as a HIS). Therefore, it is obvious that for any value of R_s between 0 and ∞, one should observe the perturbed HIS behavior of either the mushroom structure with PEC patches, $R_s = 0$, or the structure with transparent patches, $R_s = \infty$.

To validate that the resonances observed in the mushroom HIS absorber considered in this section are the perturbed HIS resonances of the mushroom HIS structure with PEC patches, we studied the current distribution for various resistivities, with R_s varying from 0 to ∞. Fig. 11 shows the normalized wire current in the single-layer mushroom structure at $f = 7$ GHz. For small values of R_s (i.e., from 0 to 120.4 Ω) it is observed that the wire current is uniform, indicating that spatial dispersion effects are almost negligible. This is consistent with the study reported in [17], where it was shown that for large values of σ_{2D}, the current distribution is uniform (which shows that spatial dispersion is reduced; however, an ABC [17, eq. (6)], is necessary in the analytical model). Since, the values of R_s are small ($R_s = 0$ to 120.4 Ω), current distribution is uniform (similar to the case of mushroom structure with PEC patches

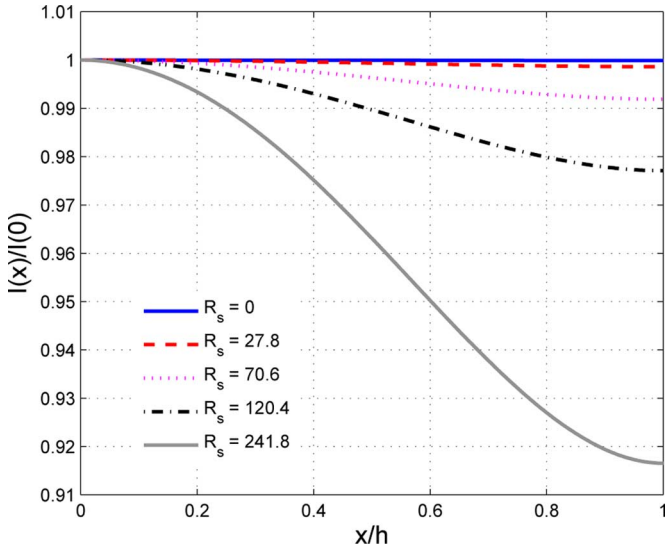

Fig. 11. Normalized wire current in the single-layer mushroom structure for different values of sheet resistivity R_s (in Ω) at $f = 7$ GHz, $\theta = 45°$.

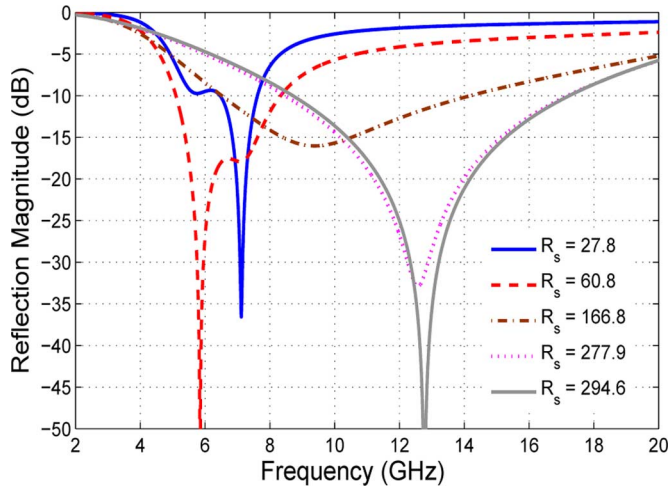

Fig. 12. Reflection magnitude of the single-layer mushroom structure for different values of sheet resistivity R_s (in Ω), $\theta = 30°$.

[14], [15]), and the phase behavior of the perturbed structure is close to that of the mushroom structure with PEC patches [blue curve in Fig. 10(a)], the resonances of the perturbed structure (absorber) observed in Fig. 10(a) [with corresponding magnitudes in Fig. 10(b)] are indeed the perturbed HIS resonances of the mushroom structure with PEC patches.

In [39], an absorber composed of PEC patches on a lossy grounded dielectric slab perforated with metallic vias was studied to enhance the absorption bandwidth for the obliquely incident plane wave. We investigated this structure using the methodology described above (i.e., the reflection properties, phase and magnitude, are analyzed with increasing losses in the dielectric slab) and in fact it is observed that the wideband absorption is due to the perturbed HIS resonances rather than to the utilization of the plasma resonance, as suggested by the authors in [39].

Since the patch arrays are the only lossy components in the absorber shown in Fig. 7, their sheet resistivity value constitutes an important factor in the performance of the absorber. Hence, selecting a proper value of R_s is the key in the design of wideband absorbers. One way of obtaining an optimum value of R_s for a wideband absorber is to use numerical optimization techniques, which is beyond the scope of this work. Given that the analytical model provides results almost instantaneously, it provides a reliable, fast, and efficient solution in selecting an optimum sheet resistance of the patch arrays. The idea is to obtain a certain range for R_s (in the range between the PEC case and wire-medium slab case) for each of the angles of incidence, where perfect reflection nulls are noticed for one of the two perturbed HIS resonances of the structure.

Fig. 12 shows the reflection coefficient for a TM-polarized plane wave incident at 30°. Starting from the case of PEC patch array (i.e., $R_s = 0$), the sheet resistivities are increased gradually up to $R_s = \infty$. Since, the reflection magnitudes for $R_s = 0$ and ∞ are 1 (i.e., 0 dB), their behavior is not shown here. It is observed that the absorption behavior takes different forms depending on the value of R_s. By varying the value of R_s one can notice the change in the absorption level of one of the reflection nulls associated with the perturbed HIS resonances (similar to the case of 45°, discussed above). Based on this observation, we fix the range for R_s where perfect reflection nulls can be obtained. From Fig. 12 it is clear that for sheet resistivities corresponding to $R_s = 60.8\ \Omega$ and 294.6 Ω, we have perfect reflection nulls at frequencies 5.845 GHz and 12.77 GHz, respectively. Hence, the range of R_s for the plane wave incident at 30° is given to be (60.8 to 294.6) Ω. A similar procedure is repeated for 45° and 60°, and the ranges for R_s are found to be (70.56–241.8) Ω and (94.03–146.38) Ω, respectively. Then, based on these values of R_s, a unique range that fits for all angles of incidence (up to 60°) can be found: (94.03–146.38) Ω for the case under study. A further optimization procedure limited to the above range gives us an optimum value of $R_s = 106.54\ \Omega$, which is the one used in the absorber design in Fig. 7.

C. Two-Layer Mushroom Structure With Thin Resistive Patches

The absorber described in Section III-B is a single-layer structure with only a few degrees of freedom available to be used for the design of an absorber over a wider range of frequencies. To improve the performance of the single-layer structure by increasing the degrees of freedom, a two-layer structure with the geometry shown in Fig. 13 is considered. The absorber consists of two resistive patch arrays separated by dielectric slabs perforated with metallic vias, with a ground plane at the bottom. For simplicity, in this work, we consider the case of wires with the same radii. The parameters of the dielectric slabs used in the design together with the dimensions and sheet resistivity values of the square patches are given in the caption of Fig. 13.

The reflection coefficient of the absorber for oblique angles of incidence obtained by the analytical model is shown in Fig. 14, and compared with the HFSS results. The comparisons illustrate the effectiveness of our model, where a good agreement is observed in the entire frequency band for all angles of incidence. In particular, it verifies the possibility of the accurate modeling of the doubled-sided wire media with thin resistive patches at the junctions, using the proposed ABCs. This would not be possible using the local model [14] (which is based on the fact that the charge build up diminishes at the wire-to-patch junctions, such that the wire-medium slab can be homogenized as a uni-

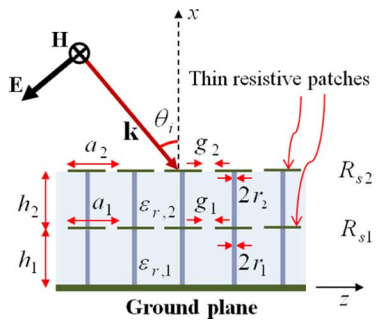

Fig. 13. Two-layer mushroom-type HIS absorber with thin resistive patches. Structural parameter used in this work: $h_1 = h_2 = 3.2$ mm, $\varepsilon_{r,1} = 2.2$, $\varepsilon_{r,2} = 1.33$, $r_1 = r_2 = 0.05$ mm, $a_1 = a_2 = 5$ mm, $g_1 = g_2 = 0.1$ mm, $R_{s1} = 196\ \Omega$, $R_{s2} = 1078\ \Omega$.

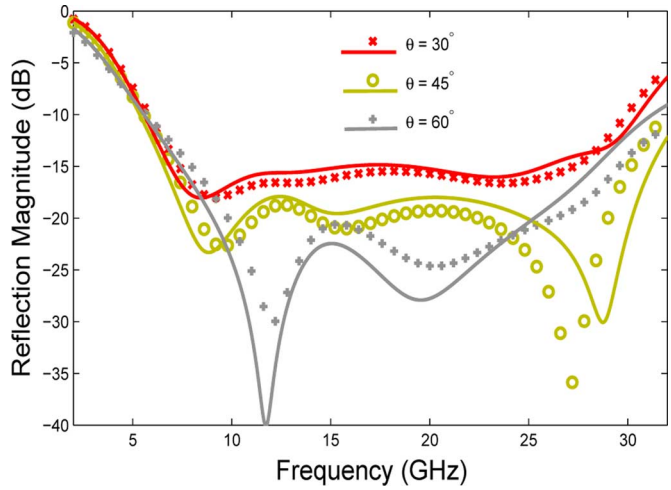

Fig. 14. Comparison of analytical (solid lines) and full-wave HFSS results (crosses, circles, and plus signs) of the reflection coefficient for the two-layer mushroom HIS absorber excited by a TM-polarized plane wave at oblique angles of incidence θ.

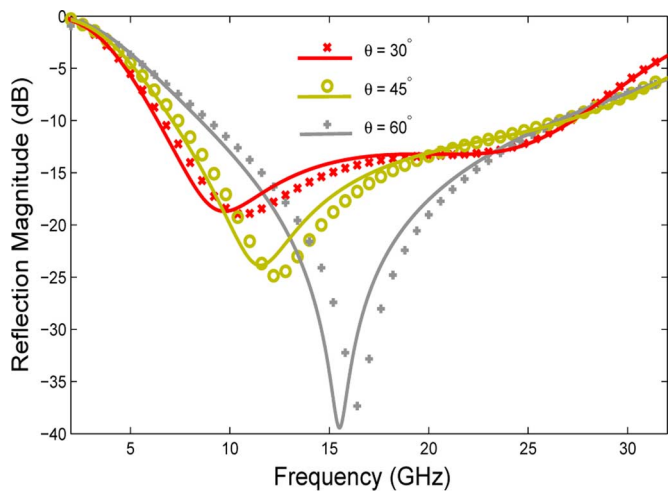

Fig. 15. Comparison of analytical (solid lines) and full-wave HFSS results (crosses, circles, and plus signs) of the reflection coefficient for the two-layer HIS absorber (without vias) excited by a TM-polarized plane wave at oblique angles of incidence θ.

axial continuous ENG material), and hence, ABCs are essential to obtain the correct results (see [17, Fig. 5]). In general, the analytical model considered in this work is valid provided the radius of the vias is much smaller than the period a and the spacing between the wires a is much smaller than the wavelength in the host medium, $k_r a \ll 2\pi$ or $a \ll \lambda_r$, where $k_r = k_0\sqrt{\varepsilon_r}$ is the wave vector, $\lambda_r = \lambda_0/\sqrt{\varepsilon_r}$ is the wavelength, and $\varepsilon_r = \varepsilon_{r,1}$, with $\varepsilon_{r,1}$ being the largest permittivity of the dielectric materials used in the two-layer mushroom structure. However, it is noticed from Fig. 14 that at the highest operational frequency 32 GHz, $a \approx 0.79\lambda_r$, and surprisingly the model still captures the physics even beyond the homogenization limit. Hence, the condition $a \ll \lambda_r$ is not necessarily required to be strictly enforced, however, it is required that a is sufficiently smaller than λ_r, provided the gap g between the patches is small, $g \ll a$. Fig. 15 shows the results of the two-layer structure without vias. Clear differences can be seen when the results of Figs. 14 and 15 are compared. In Fig. 14 we see a significant enlargement of the absorption band for oblique angles of incidence, as compared to the case of no vias (Fig. 15). Also, Fig. 14 shows that the two-layer mushroom structure, while maintaining wide bandwidths, allows for the enhancement of the absorption for increasing angles of incidence. However, for the structure with no vias, the bandwidth decreases when the absorption increases. For example, for $\theta = 60°$, it can be noticed that the 20 dB absorption bandwidth of the structure with vias covering the frequency band from 9.03 GHz to 25.29 GHz has a 55.5% bandwidth increase in comparison to the structure without vias with the frequency band from 12.67 GHz to 18.86 GHz. Furthermore, it can be observed that the relative bandwidth of absorption of the two-layer structure studied in Figs. 14 and 15 increases with respect to the single-layer structure analyzed in Figs. 8 and 9. It should be noted that, although the proposed two-layer absorber shows improvement both in bandwidth and absorption for the obliquely incident TM-polarized plane waves, there can be a number of different optimized solutions with similar wideband results as those shown in Fig. 14. Designing an absorber with optimum performance is always a challenging task because of having a large number of degrees of freedom. Hence, by proper selection of dimensions and resistivities of the patch arrays, and thicknesses and permittivities of the dielectric slabs, one can obtain a better solution (i.e., wider bandwidth and increased absorption) than the one shown in Fig. 14. The design procedure described in Section III-B for the single-layer absorber can be used to obtain the values of R_s in the design of the two-layer structure. Although this idea may seem trivial and simple to implement, the selection of the proper values of R_s in the design of a wideband absorber is a tedious process (because of increased degrees of freedom) and, hence, the explanation of the design procedure is omitted here for the sake of brevity. One can use the numerical techniques [40], [41], to obtain better optimized values of R_s, however, this is not the subject of the present paper.

In many applications it is desirable to have wideband absorption properties for both TM and TE polarizations. For TE illumination, although wideband absorption behavior is noticed, the stability of the absorption level decreases for increasing angles of incidences. This is due to the fact that, for TE illumination the electric field is orthogonal to the thin vertical metallic vias, and therefore the interaction will be negligible. Since the work carried out in this paper deals with the interaction of incident

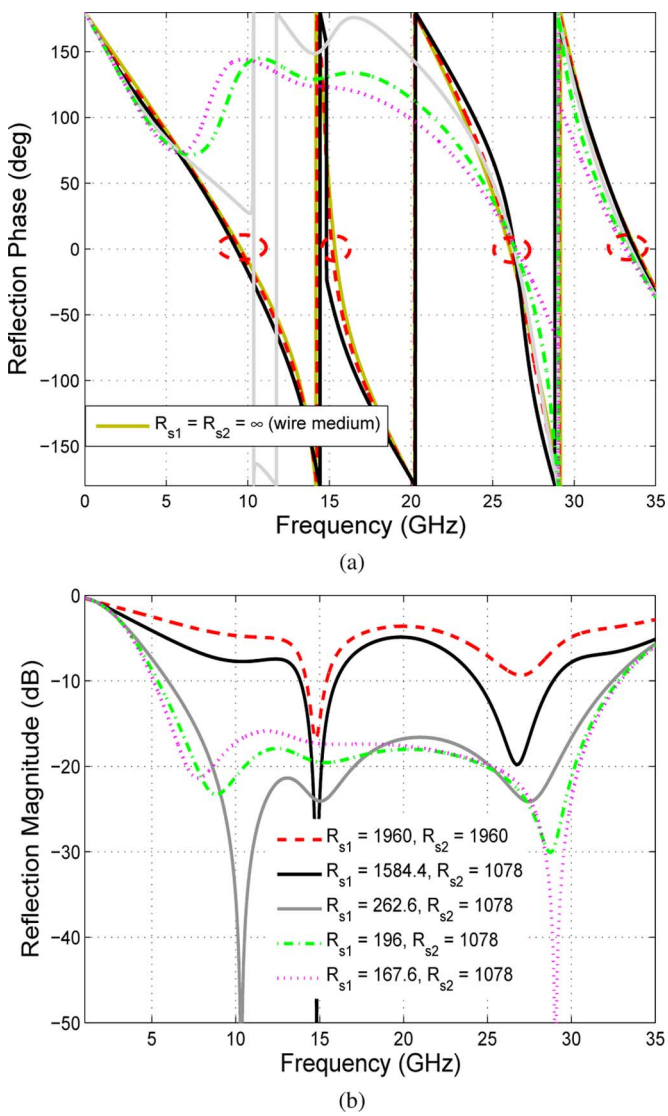

Fig. 16. (a) Phase and (b) magnitude of the reflection coefficient of the two-layer mushroom structure for different values of sheet resistivity R_s (in Ω), $\theta = 45^\circ$.

field with the vertical vias, i.e., for obliquely incident TM-polarized plane wave, the results for TE polarization are henceforth omitted.

For the single-layer structure, it was observed that the additional resonance of the mushroom structure is used to obtain wide bandwidths with enhanced absorption, and that the resonances resulting in wideband behavior are the perturbed HIS resonances of the mushroom structure with PEC patches. However, for the two-layer structure, the behavior of resonances and wide bandwidths are not due to the perturbation of the structure with PEC patches ($R_s = 0$), but due to the perturbation of the resonances of the wire-medium slab ($R_s = \infty$). To explain this we study in Fig. 16 the reflection properties (phase and magnitude) of the structure for different resistivities of the patch arrays for a TM-polarized plane wave incident at 45°. Starting with the wire-medium slab case (i.e., $R_s = \infty$), the reflection phase behavior shows four resonances (shown in red circles in Fig. 16(a) corresponding to the zero phase). The variation of resistivities of the patch arrays can be done in many ways, for example by decreasing R_s in both layers at the same time or decreasing R_s in one layer with the other layer fixed. We employ the latter strategy, because the aim is to explain the wideband behavior of the absorber with $R_{s1} = 196\ \Omega$ and $R_{s2} = 1078\ \Omega$. By gradually decreasing the resistivity of the patch array in the bottom layer (with the resistivity of the top patch array being fixed), it is noticed that the phase behavior starts to deviate from the wire-medium slab case [shown in Fig. 16(a)]. It is also observed from the magnitude behavior shown in Fig. 16(b) that the absorption levels of the reflection minima shift with decreasing values of R_s, and for some cases there are perfect reflection nulls (similar to the behavior observed in a single-layer mushroom structure) corresponding to the zero phases of the perturbed HIS resonances of the wire-medium slab. This proves the fact that the reflection minima shown in Fig. 14, for the case of $R_{s1} = 196\ \Omega$ and $R_{s2} = 1078\ \Omega$ are associated with the perturbed HIS resonances of the actual wire-medium slab. Bandwidth enhancement with respect to the single-layer mushroom structure is also observed for small angles of incidence (results not shown here). In this case, the influence of the vias is almost negligible since the electric field is almost orthogonal to the vias. The bandwidth enhancement is then explained in terms of the mutual interactions between patches printed in the adjacent layers. For higher angles of incidence, the role of vias is dominant and they are responsible for the widening of the useful frequency band. Hence, by using the resonances of the mushroom structure, along with the proper choice of dimensions and resistivities of the patch arrays, and with good selection of the permittivities of the dielectric slabs (perforated with metallic vias) the absorption bandwidth can be enlarged, as compared to the case with no vias.

The behavior of the current along the vias has also been studied for various resistivities of the patch arrays. Fig. 17 shows the normalized wire current in the two-layer mushroom structure at $f = 15$ GHz. The aim is to verify that the resonances resulting in the wideband behavior shown in Fig. 16 are actually due to the perturbation of the HIS resonances of the wire-medium slab. For the values of R_s used in Fig. 16(b), it can be observed from Fig. 17 that the current along the metallic vias varies significantly, indicating that the spatial dispersion effects are not suppressed. The reason is that when the R_s is large (conductivity is small), the thin resistive patch resembles a dielectric rather than a metal, and charges accumulate at the tip of the double-sided wire-to-patch junction, which necessitates the ABCs derived in Section II. This behavior is consistent with the study reported in [17] for small values of σ_{2D}, however, it should be noted that the structure in that paper has a single-sided wire-to-patch junction. Hence, from the behavior of the current (nonuniformity) and the phase behavior (perturbed), the resonances of the absorber are indeed the perturbed HIS resonances of the wire-medium slab.

D. Three-Layer Mushroom Structure With Thin Resistive Patches

The purpose of this section is to show that the analytical model derived in Section II can be applied to model a large number of mushroom structure layers (with double-sided wire-to-thin-resistive-patch junctions). The structure consists of three resistive patch arrays separated by dielectric slabs perforated with metallic vias, with a ground plane at the bottom

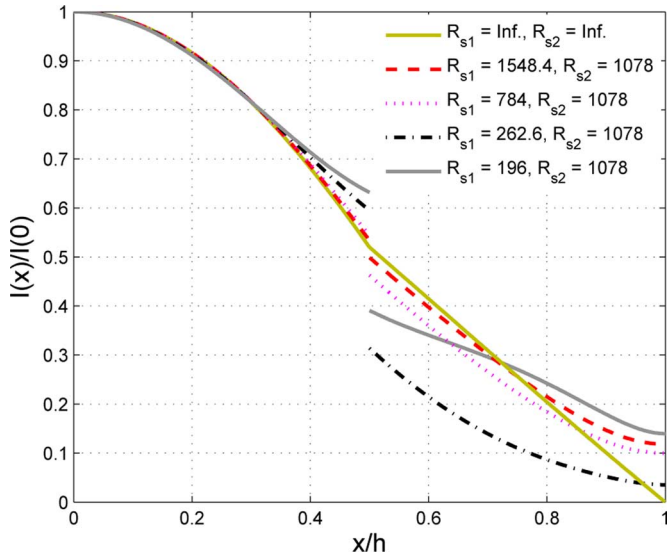

Fig. 17. Normalized wire current in the two-layer mushroom structure for different values of sheet resistivity R_s (in Ω) at $f = 15$ GHz, $\theta = 45°$. Here h is the total thickness of the two-layer structure given by $h_1 + h_2$.

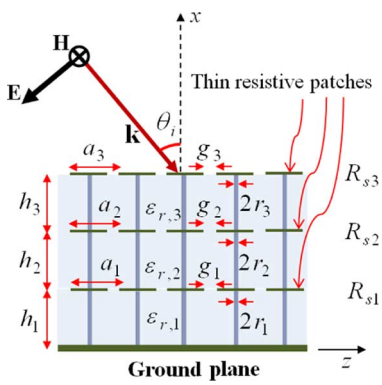

Fig. 18. Three-layer mushroom-type HIS absorber with thin resistive patches. Structural parameter used in this work: $h_1 = 2.7$ mm, $h_2 = h_3 = 3.2$ mm, $\varepsilon_{r,1} = 3.2$, $\varepsilon_{r,2} = 1.8$, $\varepsilon_{r,3} = 1.33$, $r_1 = r_2 = r_3 = 0.05$ mm, $a_1 = a_2 = a_3 = 5$ mm, $g_1 = g_2 = g_3 = 0.1$ mm, $R_{s1} = 196\ \Omega$, $R_{s2} = 588\ \Omega$, $R_{s3} = 1176\ \Omega$.

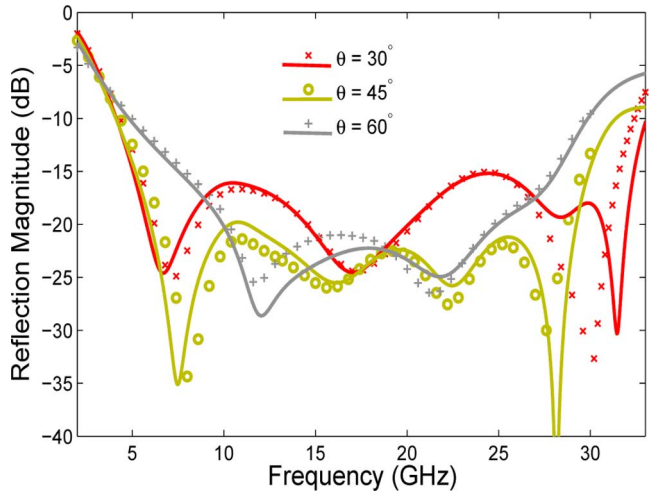

Fig. 19. Comparison of analytical (solid lines) and full-wave HFSS results (crosses, circles, and plus signs) of the reflection coefficient for the three-layer mushroom HIS absorber excited by a TM-polarized plane wave at oblique angles of incidence θ.

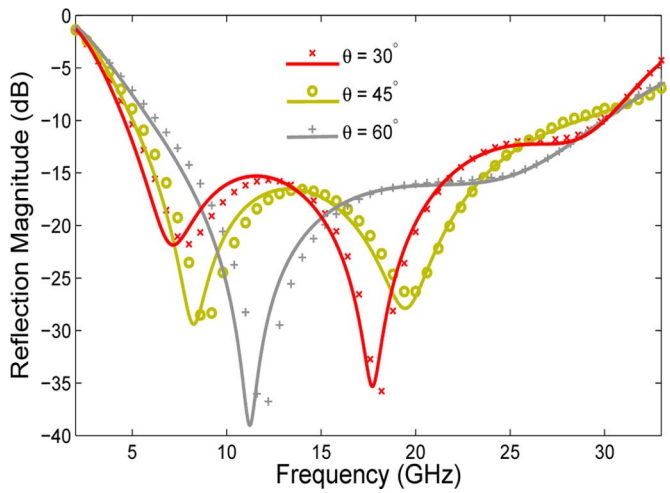

Fig. 20. Comparison of analytical (solid lines) and full-wave HFSS results (crosses, circles, and plus signs) of the reflection coefficient for the three-layer HIS absorber (without vias) excited by a TM-polarized plane wave at oblique angles of incidence θ.

(with the geometry shown in Fig. 18). The parameters of the dielectric slabs together with the dimensions and sheet resistivities of the square patches are given in the caption of Fig. 18. In Fig. 19, the magnitude of the reflection coefficient is plotted for different incidence angles. The results obtained using the analytical model described in Section II agree very well with the HFSS results. It is also observed that, as the incidence angle increases, the interaction with the vias grows and absorption is increased, as expected. Finally, Fig. 20 shows the magnitude of the reflection coefficient of the absorber without vias, with the parameters in the caption of Fig. 18. By comparing Figs. 19 and 20, one can clearly see significant improvements in the absorption bandwidth for increasing angles of incidence. For example, for $\theta = 60°$, the 20 dB absorption bandwidth of the structure with vias covering the frequency band from 9.93 GHz to 24.93 GHz shows a 38% increase in the bandwidth when comparing to the structure with no vias, having the bandwidth from 9.01 GHz to 14.6 GHz. Also, it should be noted that the HFSS results shown in Fig. 19 for $\theta = 45°$ and 60° have been obtained up to 30 GHz only (due to lack of convergence at higher frequencies). Further, it should be noted that, due to high resistivity of the top patch arrays in the two-layer and three-layer mushroom structures (i.e., with $R_{s2} = 1078\ \Omega$ in the two-layer, and $R_{s3} = 1176\ \Omega$ in the three-layer), one can replace them with solid resistive sheets with same resistive values, without causing much deviations in the absorption behavior. This is because the resistivity in these cases dominates the capacitive impedance of the patch array, and hence the gaps in these patches can be neglected.

IV. Conclusions

A simple analytical model has been presented to analyze the reflection properties of multilayered mushroom HIS structures with thin resistive patches. Additional boundary conditions for the double-sided junctions of wire media with thin resistive patches at the interface have been obtained. The limitations and applicability of the new boundary conditions have been studied, particularly for the two-layer mushroom structure, and the analytical model results have been verified using full-wave simulations. It is observed that the model gives accurate results

when $g \ll a$ for small and moderate values of the patch resistivity, however, for large values of g, the value of R_s should be large. Further, a design procedure for selecting resistivities of the patch arrays has been presented. By using the resonances of the mushroom and wire-medium HIS structures, we have shown that the absorption band can be enlarged with enhanced absorption for obliquely incident TM-polarized plane waves, when compared to the structure without vias. Also, it is observed that for the single-layer mushroom absorber (with small resistivities of the patch arrays) the resonances resulting in the wideband behavior are indeed the perturbed HIS resonances of the mushroom structure with PEC patches. However, for the two-layer structure it is observed that the resonances resulting in the wideband behavior are the perturbed resonances of the wire-medium slab.

V. Acknowledgments

The authors are thankful to the reviewers for helpful comments.

References

[1] D. R. Smith, W. J. Padilla, D. C. Vier, S. C. Nemat-Nasser, and S. Schultz, "A composite medium with simultaneously negative permeability and permittivity," *Phys. Rev. Lett.*, vol. 84, pp. 4184–4184, May 2000.

[2] M. G. Silveirinha, "Broadband negative refraction with a crossed wire mesh," *Phys. Rev. B*, vol. 79, pp. 153109(1–4)–153109(1–4), 2009.

[3] P. A. Belov, Y. Hao, and S. Sudhakaran, "Subwavelength microwave imaging in photonic crystals," *Phys. Rev. B*, vol. 73, pp. 033108(1–4)–033108(1–4), 2006.

[4] M. G. Silveirinha, P. A. Belov, and C. R. Simovski, "Subwavelength imaging at infrared frequencies using an array of metallic nanorods," *Phys. Rev. B*, vol. 75, pp. 035108(1–12)–035108(1–12), 2007.

[5] P. A. Belov, R. Marqués, S. I. Maslovski, I. S. Nefedov, M. G. Silveirinha, C. R. Simovski, and S. A. Tretyakov, "Strong spatial dispersion in wire media in the very large wavelength limit," *Phys. Rev. B*, vol. 67, pp. 113103(1–4)–113103(1–4), 2003.

[6] L. Landau and E. Lifchitz, "Electrodynamics of continuous media," in *Course of Theoretical Physics*, 2nd ed. Burlington, MA: Butterworth-Heinemann, 1984, vol. 8.

[7] M. G. Silveirinha, C. A. Fernandes, and J. R. Costa, "Electromagnetic characterization of textured surfaces formed by metallic pins," *IEEE Trans. Antennas Propagat.*, vol. 56, no. 2, pp. 405–415, Feb. 2008.

[8] M. G. Silveirinha, C. A. Fernandes, and J. R. Costa, "Additional boundary condition for a wire medium connected to a metallic surface," *New J. Phys.*, vol. 10, pp. 053011(1–17)–053011(1–17), 2008.

[9] M. G. Silveirinha, "Additional boundary condition for the wire medium," *IEEE Trans. Antennas Propagat.*, vol. 54, pp. 1766–1780, 2006.

[10] S. I. Maslovski, T. A. Morgado, M. G. Silveirinha, C. S. R. Kaipa, and A. B. Yakovlev, "Generalized additional boundary conditions for wire media," *New J. Phys.*, vol. 12, pp. 113047(1–19)–113047(1–19), 2010.

[11] M. G. Silveirinha and A. B. Yakovlev, "Negative refraction by a uniaxial wire medium with suppressed spatial dispersion," *Phys. Rev. B*, vol. 81, pp. 233105(1–4)–233105(1–4), 2010.

[12] D. Sievenpiper, L. Zhang, R. Broas, N. Alexopoulos, and E. Yablonovitch, "High-impedance electromagnetic surfaces with a forbidden frequency band," *IEEE Trans. Microw. Theory Tech.*, vol. 47, no. 11, pp. 2059–2074, Nov. 1999.

[13] A. Demetriadou and J. B. Pendry, "Taming spatial dispersion in wire metamaterial," *J. Phys., Condens. Matter*, vol. 20, pp. 295222–295222, 2008.

[14] O. Luukkonen, M. G. Silveirinha, A. B. Yakovlev, C. R. Simovski, I. S. Nefedov, and S. A. Tretyakov, "Effects of spatial dispersion on reflection from mushroom-type artificial impedance surfaces," *IEEE Trans. Microw. Theory Tech.*, vol. 57, no. 11, pp. 2692–2699, Nov. 2009.

[15] A. B. Yakovlev, M. G. Silveirinha, O. Luukkonen, C. R. Simovski, I. S. Nefedov, and S. A. Tretyakov, "Characterization of surface-wave and leaky-wave propagation on wire-medium slabs and mushroom structures based on local and nonlocal homogenization models," *IEEE Trans. Microw. Theory Tech.*, vol. 57, no. 11, pp. 2700–2714, Nov. 2009.

[16] C. S. R. Kaipa, A. B. Yakovlev, and M. G. Silveirinha, "Characterization of negative refraction with multilayered mushroom-type metamaterials at microwaves," *J. Appl. Phys.*, vol. 109, pp. 044901(1–10)–044901(1–10), 2008.

[17] A. B. Yakovlev, Y. R. Padooru, G. W. Hanson, A. Mafi, and S. Karbasi, "A generalized additional boundary condition for mushroom-type and bed-of-nails-type wire media," *IEEE Trans. Microw. Theory Tech.*, vol. 59, no. 3, pp. 527–532, Mar. 2011.

[18] W. W. Salisbury, "Absorbent Body of Electromagnetic Waves," U.S. Patent 2,599,944, 1952.

[19] L. J. D. Toit, "The design of Jauman absorbers," *IEEE Antennas Propagat. Mag.*, vol. 36, no. 6, pp. 17–25, 1994.

[20] N. I. Landy, S. Sajuyigbe, J. J. Mock, D. R. Smith, and W. J. Padilla, "Perfect metamaterial absorber," *Phys. Rev. Lett.*, vol. 100, pp. 207402–207402, Jan. 2008.

[21] B. Wang, T. Koschny, and C. M. Soukoulis, "Wide-angle and polarization-independent chiral metamaterial absorber," *Phys. Rev. B*, vol. 80, pp. 033108(1–4)–033108(1–4), 2009.

[22] M. Diem, T. Koschny, and C. M. Soukoulis, "Wide-angle perfect absorber/thermal emitter in the terahertz regime," *Phys. Rev. B*, vol. 79, pp. 033101(1–4)–033101(1–4), 2009.

[23] H. Tao, C. M. Bingham, A. C. Strikwerda, D. Pilon, D. Shrekenhamer, N. I. Landy, K. Fan, X. Zhang, W. J. Padilla, and R. D. Averitt, "Highly flexible wide angle of incidence terahertz metamaterial absorber: Design, fabrication, and characterization," *Phys. Rev. B*, vol. 78, pp. 241103(1–4)–241103(1–4), 2008.

[24] N. I. Landy, C. M. Bingham, T. Tyler, N. Jokerst, D. R. Smith, and W. J. Padilla, "Design, theory, and measurement of a polarization-insensitive absorber for terahertz imaging," *Phys. Rev. B*, vol. 79, pp. 125104(1–6)–125104(1–6), 2009.

[25] X. Liu, T. Starr, A. F. Starr, and W. J. Padilla, "Infrared spatial and frequency selective metamaterial with near-unity absorbance," *Phys. Rev. Lett.*, vol. 104, pp. 207403–207403, May 2010.

[26] Y. Avitzour, Y. A. Urzhumov, and G. Shvets, "Wide-angle infrared absorber based on a negative-index plasmonic metamaterial," *Phys. Rev. B*, vol. 79, pp. 045131(1–5)–045131(1–5), 2009.

[27] J. Hao, J. Wang, X. Liu, W. J. Padilla, L. Zhou, and M. Qiu, "High performance optical absorber based on a plasmonic metamaterial," *Appl. Phys. Lett.*, vol. 96, pp. 251104–251104, 2010.

[28] F. Bilotti, A. Toscano, K. B. Alici, E. Ozbay, and L. Vegni, "Design of miniaturized narrowband absorbers based on resonant magnetic inclusions," *IEEE Trans. Electromagn. Compat.*, vol. 53, pp. 63–72, 2011.

[29] N. Engheta, "Thin absorbing screens using metamaterial surfaces," in *Proc. IEEE Int. Symp. Antennas Propagat.*, San Antonio, TX, 2002, vol. 2, pp. 392–395.

[30] S. Simms and V. Fusco, "Thin absorber using artificial magnetic ground plane," *Electron. Lett.*, vol. 41, no. 24, pp. 1311–1313, 2005.

[31] H. Mosallaei and K. Sarabandi, "A one-layer ultrathin meta-surface absorber," presented at the IEEE Int. Symp. Antennas Propag., Washington, D.C., Jul. 2005.

[32] Q. Gao, Y. Yin, D.-B. Yan, and N.-C. Yuan, "A novel radar-absorbing-material based on EBG structure," *Microw. Opt. Technol. Lett.*, vol. 47, no. 3, pp. 228–230, 2005.

[33] B. A. Munk, *Frequency Selective Surfaces: Theory and Design*. New York: Wiley, 2000.

[34] B. A. Munk, P. Munk, and J. Pryor, "On designing Jaumann and circuit analog absorbers (CA absorbers) for oblique angle of incidence," *IEEE Trans. Antennas Propagat.*, vol. 55, no. 1, pp. 186–193, Jan. 2007.

[35] A. Kazemzadeh and A. Karlsson, "Capacitive circuit method for fast and efficient design of wideband radar absorbers," *IEEE Trans. Antennas Propagat.*, vol. 57, no. 8, pp. 2307–2314, Aug. 2009.

[36] A. Kazemzadeh and A. Karlsson, "Nonmagnetic ultrawideband absorber with optimal thickness," *IEEE Trans. Antennas Propagat.*, vol. 59, no. 1, pp. 135–140, Jan. 2011.

[37] A. Kazemzadeh and A. Karlsson, "Multilayered wideband absorbers for oblique angle of incidence," *IEEE Trans. Antennas Propagat.*, vol. 58, no. 11, pp. 3637–3646, Nov. 2010.

[38] S. A. Tretyakov and S. I. Maslovski, "Thin absorbing structures for all incidence angles based on the use of a high-impedance surface," *Microw. Opt. Technol. Lett.*, vol. 38, no. 2, pp. 153–157, 2003.

[39] O. Luukkonen, F. Costa, C. R. Simovski, A. Monorchio, and S. A. Tretyakov, "A thin electromagnetic absorber for wide incidence angles and both poalrizations," *IEEE Trans. Antennas Propagat.*, vol. 57, no. 10, pp. 3119–3124, Oct. 2009.

[40] L. J. D. Toit and J. H. Cloete, "Electric screen Jauman absorber design algorithms," *IEEE Trans. Microw. Theory Tech.*, vol. 44, pt. 1, pp. 2238–2245, 1996.

[41] S. Chakravarty, R. Mittra, and N. R. Williams, "Application of the microgenetic algorithm (MGA) to the design of broad-band microwave absorbers using multiple frequency selective surface screens buried in dielectrics," *IEEE Trans. Antennas Propagat.*, vol. 50, pp. 284–296, 2002.
[42] S. Datta, C. T. Chan, K. M. Ho, and C. M. Soukoulis, "Effective dielectric constant of periodic composite structures," *Phys. Rev. B*, vol. 48, pp. 14936(1–8)–14936(1–8), 1993.
[43] M. G. Silveirinha and C. A. Fernandes, "Effective permittivity of metallic crystals: A periodic Green's function formulation," *Electromagnetics*, vol. 8, pp. 647–663, 2003.
[44] M. G. Silveirinha and C. A. Fernandes, "Homogenization of metamaterial surfaces and slabs: The crossed wire mesh canonical problem," *IEEE Trans. Antennas Propagat.*, vol. 53, no. 1, pp. 59–69, Jan. 2005.
[45] M. G. Silveirinha, "Nonlocal homogenization model for a periodic array of ε-negative rods," *Phys. Rev. E*, vol. 73, pp. 046612(1–10)–046612(1–10), 2006.
[46] M. G. Silveirinha, "Additional boundary conditions for nonconnected wire media," *New J. Phys.*, vol. 11, pp. 053011(1–27)–053011(1–27), 2009.
[47] C. S. R. Kaipa, A. B. Yakovlev, S. I. Maslovski, and M. G. Silveirinha, "Indefinite dielectric response and all-angle negative refraction in a structure with deeply-subwavelength inclusions," *Phys. Rev. B*, vol. 84, pp. 165135(1–7)–165135(1–7), 2011.
[48] C. S. R. Kaipa, A. B. Yakovlev, S. I. Maslovski, and M. G. Silveirinha, "Mushroom-type high-impedance surface with loaded vias: Homogenization model and ultra-thin design," *IEEE Antennas Wireless Propagat. Lett.*, vol. 10, pp. 1503–1506, 2011.
[49] High Frequency Structure Simulator (HFSS) Ver. 12.0 Ansoft Corporation, PA, 2010 [Online]. Available: http://ansoft.com
[50] G. Hanson, "Dyadic Green's functions and guided surface waves on graphene," *J. Appl. Phys.*, vol. 103, pp. 064302(1–8)–064302(1–8), 2008.
[51] S. Tretyakov, *Analytical Modeling in Applied Electromagnetics*. Norwood, MA: Artech House, 2003.
[52] O. Luukkonen, C. Simovski, G. Grant, G. Goussetis, D. Lioubtchenko, A. Raisanen, and S. Tretyakov, "Simple and accurate analytical model of planar grids and high-impedance surfaces comprising metal strips and patches," *IEEE Trans. Antennas Propagat.*, vol. 56, no. 6, pp. 1624–1632, Jun. 2008.
[53] C. S. R. Kaipa, A. B. Yakovlev, F. Medina, F. Mesa, C. A. M. Butler, and A. P. Hibbins, "Circuit modeling of the transmissivity of stacked two-dimensional metallic meshes," *Opt. Exp.*, vol. 18, no. 13, pp. 13309(1–12)–13309(1–12), 2010.
[54] Y. R. Padooru, A. B. Yakovlev, C. S. R. Kaipa, F. Medina, and F. Mesa, "Circuit modeling of multi-band high-impedance surface absorbers in the microwave regime," *Phys. Rev. B*, vol. 84, pp. 035108(1–11)–035108(1–11), 2011.

Yashwanth R. Padooru (S'08) was born in Hyderabad, India, in 1985. He received the Bachelors degree in electronics and communication engineering from the Jawaharlal Nehru Technological University, Hyderabad, India, in 2006, the M.S.E.E. degree from the University of Mississippi, University, in 2009, and is currently working toward the Ph.D. degree in electrical engineering at The University of Mississippi.

He is currently a Research Assistant with the Department of Electrical Engineering, The University of Mississippi. His research interests include electromagnetic wave propagation in periodic structures, design of wideband absorbers, and modeling of cloaking structures.

Alexander B. Yakovlev (S'94–M'97–SM'01) received the Ph.D. degree in radiophysics from the Institute of Radiophysics and Electronics, National Academy of Sciences, Kiev-30, Ukraine, in 1992, and the Ph.D. degree in electrical engineering from the University of Wisconsin at Milwaukee, in 1997.

In 2000, he joined the Department of Electrical Engineering at the University of Mississippi, University, as an Assistant Professor, and became an Associate Professor in 2004. His research interests include mathematical methods in applied electromagnetics, homogenization models for metamaterials, artificial impedance surfaces, and electromagnetic band-gap structures, theory of leaky waves, and catastrophe and bifurcation theories.

Dr. Yakovlev received the Young Scientist Award at the 1992 URSI International Symposium on Electromagnetic Theory, Sydney, Australia, and the Young Scientist Award at the 1996 International Symposium on Antennas and Propagation, Chiba, Japan. From 2003 to 2006, he was an Associate Editor-in-Chief of the *ACES Journal* and from 2005 to 2008 he was an Associate Editor of the IEEE TRANSACTIONS ON MICROWAVE THEORY AND TECHNIQUES. He is a Member of URSI Commission B. He is coauthor of the book *Operator Theory for Electromagnetics: An Introduction*, Springer, NY, 2002.

Chandra S. R. Kaipa (S'08) was born in Hyderabad, India, in 1984. He received the Bachelors degree in electronics and communication engineering from the Visvesvaraya Technological University, Belgaum, India, in 2005, the M.S.E.E. and Ph.D. degrees from the University of Mississippi, University, in 2009 and 2012, respectively.

From 2009 to 2012 he was a research assistant with the Department of Electrical Engineering, The University of Mississippi. His research interests include electromagnetic wave interaction with complex media, metamaterials, periodic structures, and layered media.

George W. Hanson (S'85–M'91–SM'98–F'09) was born in Glen Ridge, NJ, in 1963. He received the B.S.E.E. degree from Lehigh University, Bethlehem, PA, the M.S.E.E. degree from Southern Methodist University, Dallas, TX, and the Ph.D. degree from Michigan State University, East Lansing, in 1986, 1988, and 1991, respectively.

From 1986 to 1988 he was a development engineer with General Dynamics, Fort Worth, TX, where he worked on radar simulators. From 1988 to 1991 he was a research and teaching assistant in the Department of Electrical Engineering at Michigan State University. He is currently Professor of Electrical Engineering and Computer Science at the University of Wisconsin at Milwaukee. His research interests include nanoelectromagnetics, mathematical methods in electromagnetics, electromagnetic wave phenomena in layered media, integrated transmission lines, waveguides, and antennas, and leaky wave phenomena.

Dr. Hanson is a member of URSI Commission B, Sigma Xi, and Eta Kappa Nu, and was an Associate Editor for the IEEE TRANSACTIONS ON ANTENNAS AND PROPAGATION from 2002–2007. In 2006 he received the S.A. Schelkunoff Best Paper Award from the IEEE Antennas and Propagation Society. He is coauthor of the book *Operator Theory for Electromagnetics: An Introduction*, Springer, NY, 2002, and author of *Fundamentals of Nanoelectronics*, Prentice-Hall, Englewood Cliffs, NJ, 2007.

Francisco Medina (M'90–SM'01–F'10) was born in Puerto Real, Cádiz, Spain, in November 1960. He received the Licenciado and Doctor degrees from the University of Seville, Seville, Spain, in 1983 and 1987 respectively, both in physics.

From 1986 to 1987, he worked at the Laboratoire de Microondes de l'ENSEEIHT, Toulouse, France, as the recipient of a Spanish Ministry of Science and Education Research Scholarship. From 1985 to 1989, he was an Assistant Professor with the Department of Electronics and Electromagnetism, University of Seville, where, since 1990, he has been an Associate Professor of Electromagnetism. He is currently a Full Professor of Electromagnetism (since July, 2009) and Head of the Microwaves Group. His research interest includes analytical and numerical methods for guiding, resonant, and radiating structures, passive planar circuits, periodic structures, and the influence of anisotropic materials (including microwave ferrites) on such systems. He is also interested on artificial media modeling, periodic structures and extraordinary transmission phenomena.

Dr. Medina is on the Editorial Board of the *International Journal of RF and Microwave Computer-Aided Engineering*. He is a reviewer of the IEEE

TRANSACTIONS ON MICROWAVE THEORY AND TECHNIQUES and of many other IEEE, Institution of Electrical Engineers (IEE), U.K., and American Physics Society journals. He has been a member of the Technical Program Committees (TPC) of several major international and local conferences and has organized a few conferences and workshops. He is a Fellow of the Massachusetts Institute of Technology (MIT) Electromagnetics Academy.

Francisco Mesa (M'93–SM'11) was born in Cádiz, Spain, in April 1965. He received the Licenciado and Doctor degrees in physics from the University of Seville, Seville, Spain, in 1989 and 1991, respectively.

He is currently a Professor with the Department of Applied Physics 1, University of Seville. His research interests focus on electromagnetic propagation/radiation in planar structures.

Allen W. Glisson (S'71–M'78–SM'88–F'02) received the B.S., M.S., and Ph.D. degrees in electrical engineering from the University of Mississippi, University, in 1973, 1975, and 1978, respectively.

In 1978, he joined the faculty of the University of Mississippi. He is Chair Emeritus and Professor Emeritus of Electrical Engineering at the University of Mississippi.

Dr. Glisson is a Fellow of the Applied Computational Electromagnetics Society, and a member of Commission B of the International Union of Radio Science. He has received a best paper award from the SUMMA Foundation and twice received a citation for excellence in refereeing from the American Geophysical Union. He was selected as the Outstanding Engineering Faculty Member in 1986, 1996, and 2004. He received a Ralph R. Teetor Educational Award in 1989 and in 2002 he received the Faculty Service Award in the School of Engineering. He was a recipient of the 2004 Microwave Prize awarded by the Microwave Theory and Techniques Society and received the 2006 Best Paper Award from the Applied Computational Electromagnetics Society Journal. He served as the Associate Editor for Book Reviews and Abstracts for the IEEE Antennas and Propagation Society Magazine from 1984 until 2006. He currently serves on the Treasurer of the Applied Computational Electromagnetics Society. He has previously served as a member of the IEEE Antennas and Propagation Society Administrative Committee, as the secretary of Commission B of the U.S. National Committee of URSI, as an Associate Editor for *Radio Science*, as Co-Editor-in-Chief of the *Applied Computational Electromagnetics Society Journal*, and as the Editor-in-Chief of the IEEE TRANSACTIONS ON ANTENNAS AND PROPAGATION.